MOX–Report No. 01/2007

An effective fluid-structure interaction formulation for vascular dynamics by generalised Robin conditions

Fabio Nobile, Christian Vergara

MOX, Dipartimento di Matematica "F. Brioschi"
Politecnico di Milano, Via Bonardi 29 - 20133 Milano (Italy)

mox@mate.polimi.it http://mox.polimi.it

An effective fluid-structure interaction formulation for vascular dynamics by generalized Robin conditions

F. Nobile, C. Vergara

MOX – Modellistica e Calcolo Scientifico
Dipartimento di Matematica "F. Brioschi"
Politecnico di Milano
via Bonardi 9, 20133 Milano, Italy
<fabio.nobile, christian.vergara>@mate.polimi.it

Abstract

In this work we focus on the modelling and numerical simulation of the fluid-structure interaction mechanism in vascular dynamics. We first propose a simple membrane model to describe the deformation of the arterial wall, which is derived from the Koiter's shell equations and is applicable to an arbitrary geometry. Secondly, we consider a reformulation of the fluid-structure problem, in which the newly derived membrane model, thanks to its simplicity, is embedded into the fluid equations and will appear as a *generalized Robin boundary condition*. The original problem is then reduced to the solution of subsequent fluid equations defined on a moving domain and may be achieved with a fluid solver, only. We also derive a stability estimate for the resulting numerical scheme. Finally, we propose new outflow absorbing boundary conditions, which are easy to implement and allow to reduce significantly the spurious pressure wave reflections that typically appear in artificially truncated computational domains. We present several numerical results showing the effectiveness of the proposed approaches.

Keywords: Fluid-Structure Interaction, Membrane Model, Absorbing Boundary Conditions, Navier-Stokes Eqs., Womersley Profile, Finite Elements, Time Marching Schemes.

AMS Subject Classification: 74F10, 57N16, 65M60

1 Introduction

Since the early 80's, there has been a great interest in solving fluid-structure interaction problems, appearing in several engineering and biomedical applica-

tions. In particular, fluid-structure interaction mechanisms are of great importance in haemodynamics since they are responsible for pressure wave propagation from the heart to peripheral vessels and capillaries. Moreover, the deformation of the arterial wall during a cardiac beat can reach up to 10% of the artery radius and should not be neglected. This renders the coupled problem highly non-linear since the position of the fluid-structure interface is itself an unknown.

In the last few years, there has been an increasing effort to devise efficient numerical algorithms for fluid-structure simulations in haemodynamics. The most common approach consists in the subsequent solutions of the fluid and structure subproblems and allows one to couple different solvers, thus reusing available computational codes. Within this framework, *explicit* algorithms (also called loosely coupled strategies) solve the fluid and the structure only once (or just few times) per time step and do not satisfy exactly the coupling conditions (namely the continuity of velocity and normal stress at the fluid-structure interface) at each time step. As a consequence, the work exchanged between the two subproblems is not perfectly balanced and this may induce instabilities in the numerical scheme. Indeed, it was shown in [6] (see also [22]) that explicit couplings do not work in vascular dynamics because of the high added mass effect. Alternatively, one could treat implicitly the coupling conditions at each time step (*implicit* algorithms), leading to a fully coupled, monolithic system of highly non-linear equations. The monolithic problem is then solved via subiterations between the fluid and structure subproblems. Several substructuring strategies have been investigated so far, see e.g. [8, 11, 24, 35, 7, 36, 10]. In this case, the work exchanged between the two subproblems is perfectly balanced and the numerical scheme is stable. Yet, the price to pay is a relatively large number of subiterations, particularly in those cases where the added mass is important, as in haemodynamics. Up to now, the computational cost remains extremely high. The need to reduce the computational cost for haemodynamic fluid-structure simulations, has motivated this work.

The first goal of the paper is to propose a simple structure model, which is well suited to describe artery dynamics. The model is based on the assumption that the structure is thin, behaves as a *membrane* and deforms mainly in the normal direction to the mean surface. These assumptions are sound and widely accepted in vascular dynamics (see e.g. [2, 37, 41, 30]). The model is derived from the Koiter's shell equation (see [32, 33]), neglecting bending terms and transversal displacements while including pre-stresses which might actually appear in arteries. It can be written for an arbitrary surface and generalizes the so called *independent rings* and *generalized string* models, which have been derived for cylindrical surfaces upon the assumption of normal displacements (see e.g. [43, 19, 20]) and have been widely adopted in the bioengineering community. While being very simple, these models allow to reproduce important fluid-structure mechanisms that appear in haemodynamics, such as the propagation of pressure waves. The fact that our new model is applicable to an arbitrary surface and retains the same simplicity of the generalized string model, makes

it very attractive for realistic haemodynamic applications.

The second goal of the paper is to develop an efficient fluid structure coupling strategy. To this aim we propose a reformulation of the problem, in which the newly derived membrane model, thanks to its simplicity, is easily embedded into the fluid equations and will appear as a *generalized Robin boundary condition*. By doing this, the coupling fluid-structure conditions are automatically treated in an implicit way, thus preserving the stability of the numerical scheme. The resulting fluid problem remains non linear since the interface position is unknown. In this work, we propose and compare two strategies to deal with such non-linearity. The first one (hereafter called *explicit Robin scheme*) treats in an explicit way the interface position, by extrapolation from previous time steps, and does not require any subiteration. The second one (*implicit Robin scheme*) treats implicitly the interface position by fixed point subiterations. In both cases, the simulation of the original fluid structure problem reduces to the solution of subsequent fluid problems in ALE formulation ([31, 9]) with generalized Robin boundary conditions and may be achieved with only a fluid solver which includes such features.

We also provide an original stability analysis showing that, for the chosen (implicit) time discretization, both the explicit Robin and the implicit Robin strategies lead to an unconditionally stable scheme. In particular, we stress that the explicit treatment of the interface position does not affect the stability of the numerical discretization. Moreover, preliminary numerical results, show that the solutions of the explicit and of the implicit Robin schemes are in excellent agreement. Therefore, the implicit treatment of the interface position does not seem to improve substantially the numerical solution. The explicit Robin scheme is then preferable being computationally cheaper.

We point out that the idea of embedding the structure equation into the fluid has already been considered in [12], although in this work the authors do not move the fluid domain.

The structure model and the numerical scheme proposed in this work have been developed in the context of haemodynamic applications. Yet, they may be of interest also for other types of applications, whenever a fluid interacts with a thin membrane.

The proposed schemes offer also another advantage: in haemodynamic applications, it is often useful to be able to prescribe flow rate defective boundary conditions. This problem has been recently investigated in [14, 47, 48] for a rigid vessel, with a Lagrange multiplier approach. By employing the Robin schemes, the flow rate problem can be straightforwardly extended to a compliant domain.

The last topic of this paper concerns the proper choice of outflow boundary conditions for the fluid-structure problem. As we mentioned earlier, the fluid-structure mechanism in vascular dynamics gives rise to pressure waves propagating along the vessels. Hence, at the numerical level, proper absorbing boundary conditions should be prescribed at the outlet sections to avoid spurious reflections. A possible way to overcome this difficulty has been proposed in [13] and

further investigated in [15]. It consists in coupling the fluid structure 3D problem with a reduced one-dimensional model, acting as a non-reflecting boundary condition. Inspired by this *geometrical multiscale approach*, in this paper we propose a new *absorbing boundary condition* which is applied directly to the fluid problem thus avoiding the complexity of the coupling with the reduced 1D solver. This strategy is very appealing for practical haemodynamics applications and so far has produced very good results, as shown by the numerical tests presented in Section 7.

The outline of the paper is as follows. In Section 2 we derive the simple membrane model. In Section 3 we present the formulation of the fluid problem in ALE coordinates and we write the weak formulation of the coupled fluid-structure problem. In Section 4 we introduce the Robin schemes, in particular the explicit Robin algorithm and its implicit counterpart and we prove a stability result. In Section 5 we present the flow rate problem for incompressible fluids in compliant domains, while in Section 6 we propose the new absorbing boundary conditions. Finally, in Section 7, we present some numerical results.

2 Derivation of a simple linear membrane model

We assume that the structure behaves as a membrane, i.e. a thin elastic shell with no bending, whose thickness is neglected and which can be therefore described by a 2D manifold. Moreover, we assume that no shear stresses act on the membrane. This implies, in particular, that sections normal to the reference surface Γ^0 remain normal after deformation.

2.1 Inertial-algebraic model

In this section we derive a simple inertial-algebraic membrane model, considering small deformations, starting from the Koiter's model for a membrane without shear (see [32, 33]) and making further simplifying assumptions.

The reference position Γ^0 of the membrane is identified by a regular mapping

$$\boldsymbol{\phi} : \omega \subset \mathbb{R}^2 \to \Gamma^0 \subset \mathbb{R}^3, \quad \boldsymbol{\phi} = \boldsymbol{\phi}(\xi_1, \xi_2), \ \forall (\xi_1, \xi_2) \in \omega.$$

The mapping $\boldsymbol{\phi}$ introduces a local system of curvilinear coordinates, whose covariant basis is given by

$$\boldsymbol{a}_\alpha = \frac{\partial \boldsymbol{\phi}}{\partial \xi_\alpha}, \ \alpha = 1, 2, \qquad \boldsymbol{a}_3 = \frac{\boldsymbol{a}_1 \times \boldsymbol{a}_2}{|\boldsymbol{a}_1 \times \boldsymbol{a}_2|}.$$

In the sequel, we use greek letters for indices taking their values in the set $\{1, 2\}$, while latin letters for indices taking their values in the set $\{1, 2, 3\}$. The vectors $\boldsymbol{a}_1$ and $\boldsymbol{a}_2$ define the tangent plane to Γ^0 in the point (ξ_1, ξ_2) and $\boldsymbol{a}_3$ is the normal unit vector to this plane (see Figure 1). We assume that the mapping $\boldsymbol{\phi}$

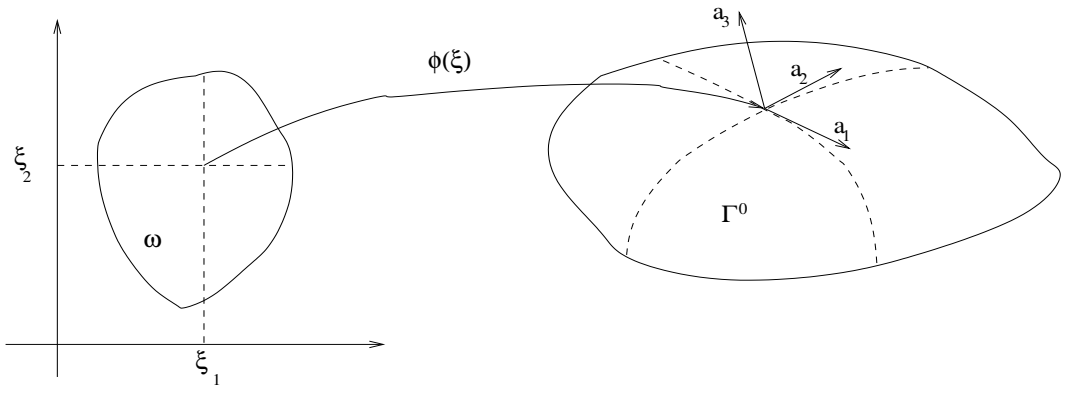

Figure 1: The regular mapping $\boldsymbol{\phi}$.

is regular, i.e. the two vectors $\boldsymbol{a}_1$ and $\boldsymbol{a}_2$ are linearly independent in all points $(\xi_1, \xi_2) \in \bar{\omega}$. We denote by

$$A_{\alpha\beta} = A_{\beta\alpha} = \boldsymbol{a}_\alpha \cdot \boldsymbol{a}_\beta, \qquad B_{\alpha\beta} = B_{\beta\alpha} = -\boldsymbol{a}_\alpha \cdot \frac{\partial \boldsymbol{a}_3}{\partial \xi_\beta} = \boldsymbol{a}_3 \cdot \frac{\partial \boldsymbol{a}_\beta}{\partial \xi_\alpha}$$

the first and the second fundamental forms of the surface Γ^0, respectively (see, e.g., [34, 1]). We also denote by $A^{\alpha\beta}$ the inverse of the matrix $A_{\alpha\beta}$ and by

$$\boldsymbol{a}^\alpha = A^{\alpha\beta}\boldsymbol{a}_\beta, \quad \boldsymbol{a}^3 = \boldsymbol{a}_3,$$

the contravariant curvilinear basis. Here and in what follows, we will adopt Einstein's convention that repeated indices are summed. In a similar manner, given a tensor $C_{\alpha\beta}$ we define $C^\lambda_\beta = A^{\alpha\lambda}C_{\alpha\beta}$. Then, any vector $\boldsymbol{v} \in \mathbb{R}^3$ can be represented in covariant or in contravariant components as $\boldsymbol{v} = v_i\boldsymbol{a}^i = v^i\boldsymbol{a}_i$. Finally, we introduce the surface covariant derivative of a vector field $\boldsymbol{v}$, defined as

$$\boldsymbol{v}^s_{\alpha/\lambda} = \frac{\partial v_\alpha}{\partial \xi_\lambda} - \Gamma^\beta_{\alpha\lambda} v_\beta, \quad \Gamma^\beta_{\alpha\lambda} = \boldsymbol{a}^\beta \cdot \frac{\partial \boldsymbol{a}_\lambda}{\partial \xi_\alpha},$$

where $\Gamma^\beta_{\alpha\lambda}$ are the Christoffel symbols (see e.g. [34, 1]).

The simplified model we will consider in this work relies on the following assumptions:

h1) linear constitutive stress-strain relation and isotropic-homogeneous material;

h2) small deformations;

h3) negligible bending terms (membrane deformation);

h4) only normal displacement.

We start by considering Koiter's model for small membrane deformations, neglecting the bending terms. This model is described by the following equations, written in weak form: let $\boldsymbol{\eta} : \Gamma^0 \to \mathbb{R}^3$ be the membrane displacement; then, given a forcing term $\boldsymbol{f}_s$, find $\boldsymbol{\eta}$ in a suitable functional space $\boldsymbol{K}$ such that, for all $\boldsymbol{\chi} \in \boldsymbol{K}$

$$\int_{\Gamma^0} \rho_s h_s \frac{\partial^2 \boldsymbol{\eta}}{\partial t^2} \cdot \boldsymbol{\chi}\, d\gamma + \int_{\Gamma^0} h_s E^{\alpha\beta\lambda\delta} \gamma_{\alpha\beta}(\boldsymbol{\eta}) \gamma_{\lambda\delta}(\boldsymbol{\chi})\, d\gamma = \int_{\Gamma^0} \boldsymbol{f}_s \cdot \boldsymbol{\chi}\, d\gamma,$$

where ρ_s and h_s are the density and the thickness of the structure, respectively. Moreover, $\gamma_{\alpha\beta}$ is the *change of metric* tensor defined by

$$\gamma_{\alpha\beta}(\boldsymbol{\chi}) = \frac{1}{2}(\chi^s_{\alpha/\beta} + \chi^s_{\beta/\alpha}) - B_{\alpha\beta}\chi_3$$

and $E^{\alpha\beta\lambda\delta}$ is the elastic tensor, given by

$$E^{\alpha\beta\lambda\delta} = \frac{E}{1+\nu} A^{\alpha\lambda} A^{\beta\delta} + \frac{E\nu}{1-\nu^2} A^{\alpha\beta} A^{\lambda\delta}.$$

Here, E and ν are the Young modulus and the Poisson coefficient, respectively, of the material at hand. The proper choice of the functional space $\boldsymbol{K}$ depends on the boundary conditions imposed on the displacement $\boldsymbol{\eta}$. We point out that we write the equations of the Koiter's model in the reference configuration Γ^0. Indeed it is a common practice to adopt a Lagrangian framework for the structure problems. Now, if we restrict the membrane displacements only to the normal direction, i.e. $\boldsymbol{\eta} = (0, 0, \eta_3)$, the previous model can be further simplified. Indeed, we have $\gamma_{\alpha\beta}(\boldsymbol{\chi}) = -B_{\alpha\beta}\chi_3$ and

$$\begin{aligned} E^{\alpha\beta\lambda\delta}\gamma_{\alpha\beta}(\boldsymbol{\eta})\gamma_{\lambda\delta}(\boldsymbol{\chi}) &= \frac{E}{1+\nu} A^{\alpha\lambda} A^{\beta\delta} B_{\alpha\beta} B_{\lambda\delta} \eta_3 \chi_3 + \\ &\quad + \frac{E\nu}{1-\nu^2} A^{\alpha\beta} A^{\lambda\delta} B_{\alpha\beta} B_{\lambda\delta} \eta_3 \chi_3 \\ &= \Big(\frac{E}{1+\nu} B^\lambda_\beta B^\beta_\lambda + \frac{E\nu}{1-\nu^2} B^\beta_\beta B^\lambda_\lambda \Big) \eta_3 \chi_3 \end{aligned}$$

and the structure model reduces to the simple scalar equation

$$\begin{cases} \rho_s h_s \dfrac{\partial^2 \eta_3}{\partial t^2} + \beta \eta_3 = f_s & \text{in } (0,T) \times \Gamma^0, \\ \eta_3|_{t=0} = \eta_0 & \text{in } \Gamma^0 \\ \dfrac{\partial \eta_3}{\partial t}\Big|_{t=0} = \eta_v & \text{in } \Gamma^0, \end{cases} \tag{1}$$

where

$$\beta = \beta(\xi_1, \xi_2) = \frac{h_s E}{1-\nu^2} ((1-\nu) B^\lambda_\beta B^\beta_\lambda + \nu B^\beta_\beta B^\lambda_\lambda) \tag{2}$$

and η_0 and η_v are the initial conditions. We point out that the model (1) is applicable to any surface identified by a regular mapping $\boldsymbol{\phi}$ and therefore it is of

practical interest in the applications where realistic computational domains are considered. Observe that, once we restrict the deformations to happen only in the normal direction, the final model (1) does not contain anymore differential operators in the space variables and, in particular, does not require any boundary conditions.

In the sequel we refer to model given by (1) and (2) as *inertial-algebraic model* and as *algebraic model* in the particular case $\rho_s = 0$.

2.2 The pre-stressed model

Starting from the 3D non-linear elasticity equations for a shell type domain and linearizing over a deformed configuration Ω_s of thickness h_s, given by $\Omega_s = \Gamma^0 \times [-h_s/2; h_s/2]$, a term of the form (in weak formulation)

$$\int_{\Omega_s} \nabla \boldsymbol{\eta}\, T : \nabla \boldsymbol{\chi}\, d\omega_s \tag{3}$$

adds to the other linear terms (see, e.g., [5]). T is the pre-stress tensor, i.e. the Cauchy stress tensor in the deformed configuration, while $\boldsymbol{\eta}$ here represents a small deformation from Ω_s. In haemodynamics, experimental analysis show that vessel walls are in a pre-stressed state both in the longitudinal and radial directions. In particular, when an artery is extracted from a body tends to reduce its length, whereas when a small anulus of artery is cut, it opens (see e.g. [23]).

In this section we want to enrich the model given by (1) and (2) with a term that takes into account this pre-stress. To this aim, we start from a 3D shell model including term (3) and then we reduce to the simple membrane case making the hypothesis (h1-h4) and taking the limit when the thickness h_s goes to zero.

In particular, since we are interested to derive a membrane model, we consider the following form for the pre-stress tensor in the local curvilinear basis:

$$T^{3D} = \begin{bmatrix} T & 0 \\ 0 & 0 \end{bmatrix}, \qquad \text{with} \qquad T = \begin{bmatrix} T^{11} & T^{12} \\ T^{12} & T^{22} \end{bmatrix},$$

which corresponds to only tangential stresses in Ω_s. According to the Koiter's model, the deformation field $\boldsymbol{\eta}$ in the 3D shell domain Ω_s is given by (see [3])

$$\boldsymbol{\eta} = \eta_i(\xi_1, \xi_2)\boldsymbol{a}^i - \xi_3(\eta_{3,\alpha} + B^\lambda_\alpha \eta_\lambda)\boldsymbol{a}^\alpha. \tag{4}$$

From (4) and neglecting the terms where ξ_3 appear since they are of higher order in the shell thickness h_s (this simplification is consistent with neglecting bending terms), the 3D covariant derivatives of $\boldsymbol{\eta}$ are given by

$$\begin{cases} \boldsymbol{\eta}_{\alpha/\beta} = \boldsymbol{\eta}^s_{\alpha/\beta} - B_{\alpha\beta}\eta_3, & \boldsymbol{\eta}_{\alpha/3} = -(\eta_{3,\alpha} + B^\lambda_\alpha \eta_\lambda), \\ \boldsymbol{\eta}_{3/\alpha} = \eta_{3,\alpha} + B^\lambda_\alpha \eta_\lambda, & \boldsymbol{\eta}_{3/3} = 0. \end{cases}$$

Therefore, integrating over the thickness and making the hypothesis of normal displacement, from (3) we obtain

$$\begin{cases} \displaystyle\int_{\Omega_s} \boldsymbol{\eta}_{\gamma/\alpha} T^{\alpha\beta} \boldsymbol{\chi}_{\gamma/\beta} d\omega_s = \int_{\Gamma^0} \int_{-h_s/2}^{h_s/2} B_{\gamma\alpha} \eta_3 T^{\alpha\beta} B_{\gamma\beta} \chi_3 \, dl d\gamma = \\ \qquad\qquad\qquad\qquad = \displaystyle\int_{\Gamma^0} h_s B_{\gamma\alpha} T^{\alpha\beta} B_{\gamma\beta} \eta_3 \chi_3 \, d\gamma \\ \displaystyle\int_{\Omega_s} \boldsymbol{\eta}_{3/\alpha} T^{\alpha\beta} \boldsymbol{\chi}_{3/\beta} d\omega_s = \int_{\Gamma^0} \int_{-h_s/2}^{h_s/2} \eta_{3,\alpha} T^{\alpha\beta} \chi_{3,\beta} dl d\gamma = \int_{\Gamma^0} h_s T^{\alpha\beta} \eta_{3,\alpha} \chi_{3,\beta} d\gamma. \end{cases}$$

Adding these terms to model (1), the first term gives a contribution to the coefficient β of the reaction term, while the second term gives second derivatives in space. Therefore, the membrane model with a pre-stress reduces to

$$\begin{cases} \rho_s h_s \dfrac{\partial^2 \eta_3}{\partial t^2} - \nabla \cdot (T \nabla \eta_3) + \beta_2 \eta_3 = f_s & \text{in } (0,T) \times \Gamma^0 \\ \eta_3|_{t=0} = \eta_0 & \text{in } \Gamma^0 \\ \dfrac{\partial \eta_3}{\partial t}\Big|_{t=0} = \eta_v & \text{in } \Gamma^0, \end{cases} \tag{5}$$

where

$$\beta_2 = \beta_2(\xi_1, \xi_2) = h_s \Big(\frac{E}{1-\nu^2} ((1-\nu) B^\lambda_\beta B^\beta_\lambda + \nu B^\beta_\beta B^\lambda_\lambda) + B_{\gamma\alpha} T^{\alpha\beta} B_{\delta\beta} \Big) \tag{6}$$

and where the operator ∇ has to be intended as covariant. In the sequel, we refer to (5)-(6) as *pre-stressed model*. Observe that model (5) has to be endowed with proper boundary conditions on $\partial\Gamma^0$, which could be, for instance,

$$\eta_3|_{\partial\Gamma^0} = 0$$

or

$$((T \nabla \eta_3) \cdot \boldsymbol{n}_\partial)|_{\partial\Gamma^0} = 0, \tag{7}$$

where $\boldsymbol{n}_\partial$ is the normal unit vector to $\partial\Gamma^0$. In what follows, we will consider only Neumann boundary conditions (7).

2.3 An example: cylindrical geometry

As an example, let us consider a cylindrical surface

$$\Gamma^0 = \{(x,y,z) \in \mathbb{R}^3,\ x = R\cos\theta,\ y = R\sin\theta,\ \forall \theta \in [0, 2\pi),\ z \in [0, L]\},$$

where R and L are the radius and the length of the cylinder, respectively. Therefore, the surface Γ^0 in this case is obtained through the mapping

$$\boldsymbol{\phi}(\theta, z) = [x = R\cos\theta, y = R\sin\theta, z = z]^T.$$

The covariant basis is then given by

$$\boldsymbol{a}_1 = \frac{\partial \boldsymbol{\phi}}{\partial \theta} = \begin{bmatrix} -R\sin\theta \\ R\cos\theta \\ 0 \end{bmatrix}, \quad \boldsymbol{a}_2 = \frac{\partial \boldsymbol{\phi}}{\partial z} = \begin{bmatrix} 0 \\ 0 \\ 1 \end{bmatrix}, \quad \boldsymbol{a}_3 = \begin{bmatrix} \cos\theta \\ \sin\theta \\ 0 \end{bmatrix},$$

and therefore the first and the second fundamental forms are

$$A_{\alpha\beta} = \begin{bmatrix} R^2 & 0 \\ 0 & 1 \end{bmatrix}, \quad B_{\alpha\beta} = \begin{bmatrix} -R & 0 \\ 0 & 0 \end{bmatrix}.$$

Since

$$A^{\alpha\beta} = \begin{bmatrix} 1/R^2 & 0 \\ 0 & 1 \end{bmatrix},$$

we obtain

$$B^{\alpha}_{\beta} = A^{\alpha\lambda} B_{\lambda\beta} = \begin{bmatrix} -1/R & 0 \\ 0 & 0 \end{bmatrix}$$

and therefore

$$\beta = \frac{h_s E}{1-\nu^2}((1-\nu)B^{\lambda}_{\beta}B^{\beta}_{\lambda} + \nu B^{\beta}_{\beta}B^{\lambda}_{\lambda}) = \frac{h_s E}{1-\nu^2}((1-\nu)\frac{1}{R^2} + \nu\frac{1}{R^2}) = \frac{h_s E}{1-\nu^2}\frac{1}{R^2}, \tag{8}$$

which gives the well-known *independent rings* model that has been widely used in the bioengineering literature to describe artery dynamics (see e.g. [2, 37, 41, 30, 19]). Model (1)-(2) can then be viewed as a generalization of the independent rings model to an arbitrary geometry.

Let us now consider also a pre-stress term acting on the longitudinal direction only. Therefore, we assume

$$T = \begin{bmatrix} 0 & 0 \\ 0 & T^{zz} \end{bmatrix}.$$

From $(5)_1$, we obtain the following equation

$$\rho_s h_s \frac{\partial^2 \eta_3}{\partial t^2} - \mu_s \frac{\partial^2 \eta_3}{\partial z^2} + \beta \eta_3 = f_s, \tag{9}$$

where β is given by (8) and $\mu_s = T^{zz}$. This model, called *generalized string model*, has been considered, for instance, in [43, 19, 20, 24]. Therefore, model (5)-(6) can be viewed as a generalization of the generalized string model to an arbitrary geometry.

3 The fluid and the coupled fluid-structure problem

Let us consider a Newtonian incompressible fluid flowing, at time t, in the deformable domain $\Omega^t \in \mathbb{R}^3$ depicted in Figure 2. The evolution of Ω^t is not known *a priori*, since it is determined by the interaction between the fluid and

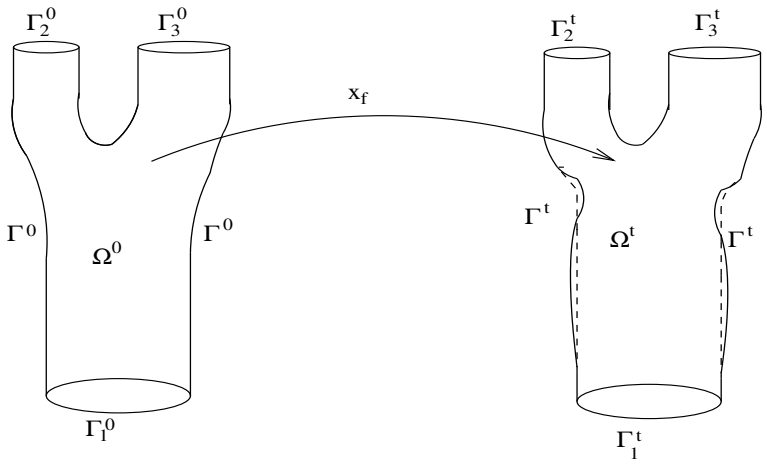

Figure 2: Reference (left) and current (right) computational domain.

the structure. The mathematical problem is therefore highly coupled and it consists in finding the velocity and the pressure of the fluid, the displacement of the structure and the position of the points of the current domain Ω^t. In what follows, we consider a geometry as depicted in Figure 2, where the solid occupies the portion Γ^t of the boundary while Γ_i^t are the fluid inflow or outflow sections.

3.1 The fluid problem

To determine the evolution of the fluid, we consider the Navier-Stokes equations for a homogeneous, incompressible, Newtonian fluid, written in ALE coordinates (see [31, 9, 16, 17, 19]). For that, we introduce a reference domain Ω^0 and a regular mapping $\boldsymbol{x}_f$ which transforms Ω^0 into the actual configuration Ω^t. The Navier-Stokes equations then read:

$$\begin{cases} \dfrac{D^A \boldsymbol{u}}{Dt} + ((\boldsymbol{u} - \widetilde{\boldsymbol{w}}) \cdot \nabla)\boldsymbol{u} - \nabla \cdot \sigma_f(\boldsymbol{u}, p) = \boldsymbol{0} & \text{in } (0,T) \times \Omega^t \\ \nabla \cdot \boldsymbol{u} = 0 & \text{in } (0,T) \times \Omega^t \\ \boldsymbol{u}|_{t=0} = \boldsymbol{u}_0 & \text{in } \Omega^t \\ \boldsymbol{u}|_{\Gamma_D^t} = \boldsymbol{g} & \text{in } (0,T) \\ (\sigma_f \widetilde{\boldsymbol{a}}_3)|_{\Gamma_N^t} = \boldsymbol{h} & \text{in } (0,T) \end{cases} \tag{10}$$

being $\boldsymbol{u} = \boldsymbol{u}(t, \boldsymbol{x})$ the fluid velocity, $p = p(t, \boldsymbol{x})$ the pressure, $\widetilde{\boldsymbol{a}}_3(t, \boldsymbol{x})$ the normal unit vector to $\partial\Omega^t$, $\boldsymbol{g}(t, \boldsymbol{x})$, $\boldsymbol{h}(t, \boldsymbol{x})$, $\boldsymbol{u}_0(\boldsymbol{x})$ given data and where

$$\sigma_f(\boldsymbol{u}, p) = \mu(\nabla \boldsymbol{u} + (\nabla \boldsymbol{u})^T) - pI$$

is the Cauchy stress tensor. We set Γ_D^t and Γ_N^t the union of the sections Γ_i^t where we impose a Dirichlet and a Neumann boundary condition, respectively. Moreover, we indicate with D^A/Dt the time derivative in ALE coordinates and

with $\widetilde{\boldsymbol{w}}$ the velocity of the points of the fluid domain in the current configuration. Let us denote by $\boldsymbol{w}$ the same quantity expressed in terms of the reference coordinate $\boldsymbol{x}^0 \in \Omega^0 : \boldsymbol{w} = \widetilde{\boldsymbol{w}} \circ \boldsymbol{x}_f$ (see Fig. 2). This quantity can be computed in an arbitrary way, provided that

$$\begin{cases} \boldsymbol{w}|_{\Gamma^t} = \boldsymbol{u}|_{\Gamma^t} \circ \boldsymbol{x}_f & \text{in } (0,T) \\ (\boldsymbol{w} \cdot \boldsymbol{a}_3)|_{\Gamma_D^0 \cup \Gamma_N^0} = 0 & \text{in } (0,T) \\ \Big(\dfrac{\partial \boldsymbol{w}}{\partial \boldsymbol{a}_3} \cdot \boldsymbol{a}_\alpha\Big)\Big|_{\Gamma_D^0 \cup \Gamma_N^0} = \boldsymbol{0}, \quad \alpha = 1,2 & \text{in } (0,T). \end{cases} \tag{11}$$

where $\boldsymbol{a}_\alpha$ are tangential unit vectors to $\partial\Omega^0$. In the sequel we will pose $\widetilde{\boldsymbol{a}}_i = \boldsymbol{a}_i \circ \boldsymbol{x}_f^{-1}$. A widely adopted method to compute the velocity $\boldsymbol{w}$ over all Ω^0, is to consider a harmonic extension operator:

$$-\triangle \boldsymbol{w} = \boldsymbol{0} \quad \text{in } (0,T) \times \Omega^0 \tag{12}$$

together with the boundary conditions (11).

Once the domain velocity is known, we can define the ALE map

$$\boldsymbol{x}_f(t, \boldsymbol{x}^0) = \boldsymbol{x}^0 + \int_0^t \boldsymbol{w}(\tau, \boldsymbol{x}^0)\, d\tau$$

which maps each point $\boldsymbol{x}^0 \in \Omega^0$ into the corresponding point of the current configuration Ω^t. The strategy based on problem (12) to compute the domain velocity might not provide an invertible (one to one) ALE mapping, if the deformation of the boundary is large and "rough". In such a case one should consider more sophisticated extensions (see e.g. [38]). Yet, in the applications we will consider in this work, strategy (12) is enough to reconstruct an admissible ALE mapping.

3.2 The coupled fluid-structure problem

We point out that problem (10) is incomplete, since we do not prescribe any condition over the interface Γ^t. This condition is determined through the coupling between the fluid and the structure model (5). To this aim, we impose the continuity of the velocity and of the normal stress at the interface Γ^t, that is

$$\begin{cases} \dfrac{\partial(\eta_3 \circ x_f^{-1})}{\partial t}\Big|_{\Gamma^t} = (\boldsymbol{u} \cdot \widetilde{\boldsymbol{a}}_3)|_{\Gamma^t} \\ (f_s \circ x_f^{-1}\delta)|_{\Gamma^t} = -((\sigma_f \widetilde{\boldsymbol{a}}_3) \cdot \widetilde{\boldsymbol{a}}_3)|_{\Gamma^t}. \end{cases} \tag{13}$$

where x_f denotes the third component of the mapping $\boldsymbol{x}_f$ and δ takes into account the change of surface area going from the reference configuration Γ^0 to the deformed one Γ^t. For example, in a cylindrical domain

$$\delta = \Big(\frac{R_0 + \eta_3}{R_0}\sqrt{1 + \Big(\frac{\partial \eta_3}{\partial z}\Big)^2 + \Big(\frac{1}{R_0 + \eta_3}\frac{\partial \eta_3}{\partial \theta}\Big)^2}\Big)^{-1},$$

where R_0 is the radius in the reference configuration and θ the angular coordinate. In order to prescribe to the fluid suitable boundary conditions at the interface also in the tangential directions, we impose

$$(\boldsymbol{u} \cdot \widetilde{\boldsymbol{a}}_\alpha)|_{\Gamma^t} = 0, \tag{14}$$

that are consistent with the fact that we are neglecting the tangential displacement of the structure.

To write the weak formulation of the coupled problem, let us consider the following functional spaces

$$\begin{cases} \boldsymbol{V}^t = \{\boldsymbol{v} \in \boldsymbol{H}^1(\Omega^t) : \boldsymbol{v}|_{\Gamma_D^t} = \boldsymbol{0} \text{ and } (\boldsymbol{v} \cdot \widetilde{\boldsymbol{a}}_\alpha)|_{\Gamma^t} = 0, \} \\ \boldsymbol{V}_{\boldsymbol{g}}^t = \{\boldsymbol{v} \in \boldsymbol{H}^1(\Omega^t) : \boldsymbol{v}|_{\Gamma_D^t} = \boldsymbol{g} \text{ and } (\boldsymbol{v} \cdot \widetilde{\boldsymbol{a}}_\alpha)|_{\Gamma^t} = 0, \} \\ Q^t = L^2(\Omega^t), \\ \boldsymbol{M}^0 = \{\boldsymbol{\psi} \in \boldsymbol{H}^1(\Omega^0) : \boldsymbol{\psi}|_{\Gamma^0} = \boldsymbol{0} \text{ and } (\boldsymbol{\psi} \cdot \boldsymbol{a}_3)|_{\Gamma_D^0 \cup \Gamma_N^0} = 0\}, \\ W^0 = H^1(\Gamma^0). \end{cases}$$

Moreover, let us introduce the following bilinear form

$$a(\boldsymbol{w}, \boldsymbol{v}) = \mu(\nabla \boldsymbol{w} + (\nabla \boldsymbol{w})^T, \nabla \boldsymbol{v}),$$

where we indicate with $(\cdot, \cdot)$ the $L^2(\Omega^t)$ inner product. Proceeding in a standard way, we recover, for each time t, the following weak formulation for the fluid problem (10) with (14): find $\boldsymbol{u} \in \boldsymbol{V}_{\boldsymbol{g}}^t$ and $p \in Q^t$, such that

$$\begin{cases} \Big(\dfrac{D^A \boldsymbol{u}}{Dt}, \boldsymbol{v}\Big) + a(\boldsymbol{u}, \boldsymbol{v}) + (((\boldsymbol{u} - \widetilde{\boldsymbol{w}}) \cdot \nabla)\boldsymbol{u}, \boldsymbol{v}) - (p, \nabla \cdot \boldsymbol{v}) = \\ \qquad\qquad = \displaystyle\int_{\Gamma^t} (\sigma_f \widetilde{\boldsymbol{a}}_3) \cdot \widetilde{\boldsymbol{a}}_3 \, (\boldsymbol{v} \cdot \widetilde{\boldsymbol{a}}_3) \, d\gamma + \int_{\Gamma_N^t} \boldsymbol{h} \cdot \boldsymbol{v} \, d\gamma \\ (q, \nabla \cdot \boldsymbol{u}) = 0 \\ \boldsymbol{u}|_{t=0} = \boldsymbol{u}_0 \end{cases} \tag{15}$$

for all $\boldsymbol{v} \in \boldsymbol{V}^t$ and $q \in Q^t$. Let us notice that, at this stage, we have not yet imposed the Dirichlet boundary condition $(13)_1$ on Γ^t, but we have left on this portion of boundary the term coming from the integration by parts. Analogously, setting $\eta = \eta_3$ and $\chi = \chi_3$, for the structure problem given by (5) with homogeneous Neumann boundary conditions, we obtain, for each time t, the following weak formulation: find $\eta \in W^0$, such that

$$\begin{cases} \rho_s h_s \Big(\dfrac{\partial^2 \eta}{\partial t^2}, \chi\Big)_{\Gamma^0} + \Big(T \nabla \eta, \nabla \chi\Big)_{\Gamma^0} + (\beta_2 \eta, \chi)_{\Gamma^0} = (f_s, \chi)_{\Gamma^0} \\ \eta|_{t=0} = \eta_0 \\ \dfrac{\partial \eta}{\partial t}\Big|_{t=0} = \eta_v \end{cases} \tag{16}$$

for all $\chi \in W^0$ and where we indicate with $(\cdot, \cdot)_{\Gamma^0}$ the $L^2(\Gamma^0)$ inner product.

Let us introduce a global weak formulation for the fluid-structure problem (see [35, 39]). Posing

$$\boldsymbol{S}^t = \{(\boldsymbol{v}, \chi) \in \boldsymbol{V}^t \times W^0 : (\boldsymbol{v} \cdot \widetilde{\boldsymbol{a}}_3 \circ \boldsymbol{x}_f)|_{\Gamma^0} = \chi\} \tag{17}$$

it is easy to check from (15), (16) and (13), that we obtain the following global formulation:

Problem 1 *Given $\boldsymbol{g} \in \boldsymbol{H}^{1/2}(\Gamma_D^t)$ and $\boldsymbol{h} \in \boldsymbol{L}^2(\Gamma_N^t)$, find $\boldsymbol{u} \in \boldsymbol{V}_{\boldsymbol{g}}^t$, $p \in Q^t$ and $\eta \in W^0$ such that, for each t,*

$$\begin{cases} \Big(\dfrac{D^A\boldsymbol{u}}{Dt}, \boldsymbol{v}\Big) + a(\boldsymbol{u}, \boldsymbol{v}) + (((\boldsymbol{u} - \widetilde{\boldsymbol{w}}) \cdot \nabla)\boldsymbol{u}, \boldsymbol{v}) - (p, \nabla \cdot \boldsymbol{v}) + \\ \qquad\qquad + \rho_s h_s \Big(\dfrac{\partial^2 \eta}{\partial t^2}, \chi\Big)_{\Gamma^0} + (T\nabla\eta, \nabla\chi)_{\Gamma^0} + (\beta_2\eta, \chi)_{\Gamma^0} = \displaystyle\int_{\Gamma_N^t} \boldsymbol{h} \cdot \boldsymbol{v}\, d\gamma \\ (q, \nabla \cdot \boldsymbol{u}) = 0 \\ \dfrac{\partial(\eta \circ \boldsymbol{x}_f^{-1})}{\partial t}\Big|_{\Gamma^t} = (\boldsymbol{u} \cdot \widetilde{\boldsymbol{a}}_3)|_{\Gamma^t} \\ \boldsymbol{u}|_{t=0} = \boldsymbol{u}_0, \qquad \dfrac{\partial \eta}{\partial t}\Big|_{t=0} = (\boldsymbol{u}_0 \cdot \boldsymbol{a}_3)|_{\Gamma^0}, \qquad \eta|_{t=0} = \eta_0 \end{cases} \tag{18}$$

for all $(\boldsymbol{v}, \chi) \in \boldsymbol{S}^t$ and $q \in Q^t$.

Observe that, thanks to the coupling condition $(13)_2$ and the particular choice (17) of the fluid-structure test functions, the two boundary terms in the fluid and in the structure problem, namely $\int_{\Gamma^t}(\sigma_f \widetilde{\boldsymbol{a}}_3) \cdot \widetilde{\boldsymbol{a}}_3\, (\boldsymbol{v} \cdot \widetilde{\boldsymbol{a}}_3)\, d\gamma$ and $(f_s, \chi)_{\Gamma^0}$, cancel perfectly.

In the next section, we will propose simple algorithms for the solution of problem (18), that can be obtained once a suitable time discretization scheme is introduced.

4 The Robin schemes

The global weak formulation (18) can be discretized in space by a finite element technique, following e.g. [39]. Concerning time discretization, several possibilities are available. Due to the high computational cost and the complexity of the fluid-structure problem, it is a common practice to adopt staggered algorithms, in which the fluid and the structure subproblems are solved separately.

In particular, *explicit* algorithms (also called loosely coupled strategies) solve the fluid and the structure only once (or just few times) per time step and do not satisfy exactly the coupling conditions (13) at each time step. As a consequence, the work exchanged between the two subproblems is not perfectly balanced and this may induce instabilities in the numerical scheme. Indeed, it was shown in [6, 22] that explicit couplings do not work in vascular dynamics because of the high added mass effect.

Alternatively, one could employ implicit time marching schemes both for the fluid and the structure terms in (18), leading to a fully coupled, monolithic system of highly non-linear equations. The monolithic problem is then solved via subiterations between the fluid and structure subproblems. Several substructuring strategies have been investigated so far, see e.g. [8, 11, 24, 35, 7, 36]. In this case, the coupling conditions are treated implicitly thus leading to stable algorithms. Yet, the price to pay is a relatively large number of subiterations, particularly in those cases where the added mass is important.

A third possibility, which has not been much exploited so far, consists in treating explicitly the position of the fluid domain, by suitable extrapolation from the information at previous time steps, while keeping the discretization of the coupling conditions (13) implicit (see [39, 27]). In this work, we will follow this approach. Moreover, thanks to the very simple structure model (1) considered, we will derive a proper formulation which allows us to embed the structure equation into the fluid problem, as a Robin-type boundary condition. Hence, the simulation of the FSI problem (10), (1), (13) reduces to the solution of fluid problems in ALE formulation with suitable Robin boundary conditions and may be achieved with only a fluid solver which has such features (*Robin scheme*). This approach can be easily extended to the structure equation (5), leading to a boundary condition at the interface that we call *generalized Robin* condition. The idea of embedding the structure equation into the fluid has already been considered in [12] although in this work the authors do not move at all the fluid domain.

We will also consider the possibility of subiterating at each time step on the position of the interface (implicit treatment of the interface). This strategy corresponds to a fixed-point algorithm and produces at convergence the solution of the monolithic problem. This approach to obtain the monolithic solution is also very attractive since, according to our preliminary results, the convergence seems to be fast also in presence of a large added mass effect (see Section 7.1).

Let us start with the case in which the interface position is treated explicitly.

4.1 Explicit treatment of the interface position (Explicit Robin scheme)

Let us consider a time discretization of the weak formulation (18). Let us set $t^n = n\Delta t$, with Δt the time step and let us consider the Implicit-Euler scheme for the fluid equation, with a semi-implicit treatment of the convective term, and an implicit first order BDF approximation for the structure equation (5), namely

$$\rho_s h_s \frac{\eta^{n+1} - 2\eta^n + \eta^{n-1}}{\Delta t^2} - \nabla \cdot (T \nabla \eta^{n+1}) + \beta_2 \eta^{n+1} = f_s^{n+1}.$$

In what follows, the superscript t will be replaced by n to indicate quantities evaluated at time t^n. Moreover, we consider an explicit treatment of the movement

of the fluid domain, solving the equations at time t^{n+1} in Ω^n, i.e. using a first order approximation. We obtain the following time discretization of problem (18): find $\boldsymbol{u}^{n+1} \in \boldsymbol{V}_{\boldsymbol{g}}^n$, $p^{n+1} \in Q^n$ and $\eta^{n+1} \in W^0$ such that, for each n,

$$\begin{cases} \dfrac{1}{\Delta t}(\boldsymbol{u}^{n+1}, \boldsymbol{v})_n + a(\boldsymbol{u}^{n+1}, \boldsymbol{v})_n + (((\boldsymbol{u}^n - \widetilde{\boldsymbol{w}}^n) \cdot \nabla)\boldsymbol{u}^{n+1}, \boldsymbol{v})_n - (p^{n+1}, \nabla \cdot \boldsymbol{v})_n + \\ \qquad + \dfrac{\rho_s h_s}{\Delta t^2}(\eta^{n+1}, \chi)_{\Gamma^0} + (T\nabla\eta^{n+1}, \nabla\chi)_{\Gamma^0} + (\beta_2\eta^{n+1}, \chi)_{\Gamma^0} = \\ \qquad = \dfrac{1}{\Delta t}(\boldsymbol{u}^n, \boldsymbol{v})_n + \displaystyle\int_{\Gamma_N^n} \boldsymbol{h} \cdot \boldsymbol{v}\, d\gamma + \dfrac{\rho_s h_s}{\Delta t^2}(2\eta^n - \eta^{n-1}, \chi)_{\Gamma^0} \\ (q, \nabla \cdot \boldsymbol{u}^{n+1})_n = 0 \\ \boldsymbol{u}^0 = \boldsymbol{u}_0, \qquad \dfrac{\partial \eta^0}{\partial t} = (\boldsymbol{u}_0 \cdot \boldsymbol{a}_3)|_{\Gamma^0}, \qquad \eta^0 = \eta_0 \end{cases} \tag{19}$$

for all $(\boldsymbol{v}, \chi) \in \boldsymbol{S}^n$ and $q \in Q^n$ and where we denote by $(\cdot, \cdot)_m$ the $L^2(\Omega^m)$ inner product. Moreover, we have denoted with $\boldsymbol{u}^m$, p^m and η^m the approximations of the exact quantities at $t = t^m$. The discretization of the second derivative in time of the structure displacement should be properly adapted at the first time step, in order to take properly into account the initial conditions. Let us also introduce a time discretization of the interface conditions $(13)_1$:

$$\frac{(\eta^{n+1} - \eta^n) \circ (\boldsymbol{x}_f^n)^{-1}}{\Delta t}\Big|_{\Gamma^n} = (\boldsymbol{u}^{n+1} \cdot \widetilde{\boldsymbol{a}}_3)|_{\Gamma^n}. \tag{20}$$

We point out that the interface condition (20) is treated implicitly, while the movement of the domain explicitly. This allows to balance properly the energy exchange between fluid and structure and obtain a stable algorithm (see Sections 4.3 and 7).

Remark 1 *The structure time discretization scheme considered in (19) (corresponding to a first order backward difference method) has been chosen for convenience, although it is highly dissipative. Second order schemes, such as the mid-point or the Houbolt one, could be considered as well.*

4.1.1 Inertial-algebraic model

Let us consider for the structure an inertial-algebraic model, i.e. problem (16) with $T = 0$ and $\beta_2 = \beta$. For the sake of simplicity, let us pose $\boldsymbol{h} = \boldsymbol{0}$ and $\boldsymbol{g} = \boldsymbol{0}$. Moreover, we adopt the shorthand notations $\sigma_3 = (\sigma_f \widetilde{\boldsymbol{a}}_3) \cdot \widetilde{\boldsymbol{a}}_3$ and, for a given function $\boldsymbol{z}$, $z_3 = \boldsymbol{z} \cdot \widetilde{\boldsymbol{a}}_3$. Let us derive the explicit Robin scheme. Thanks to (20),

from (19) and the choice of the test functions in (17), we obtain:

$$\begin{aligned}
&\Big(\frac{\boldsymbol{u}^{n+1}-\boldsymbol{u}^n}{\Delta t},\boldsymbol{v}\Big)_n + a(\boldsymbol{u}^{n+1},\boldsymbol{v})_n + (((\boldsymbol{u}^n-\widetilde{\boldsymbol{w}}^n)\cdot\nabla)\boldsymbol{u}^{n+1},\boldsymbol{v})_n + \\
&\qquad -(p^{n+1},\nabla\cdot\boldsymbol{v})_n = \\
&\qquad = -\int_{\Gamma^0}\Big(\frac{\rho_s h_s}{\Delta t^2}(\eta^{n+1}-2\eta^n+\eta^{n-1})+\beta\eta^{n+1}\Big)v_3\circ\boldsymbol{x}_f^n\,d\gamma = \\
&\qquad = -\int_{\Gamma^0}\Big(\frac{\rho_s h_s}{\Delta t}+\beta\Delta t\Big)(u_3^{n+1}\circ\boldsymbol{x}_f^n)(v_3\circ\boldsymbol{x}_f^n)\,d\gamma + \\
&\qquad\quad -\int_{\Gamma^0}\Big(\Big(-\frac{\rho_s h_s}{\Delta t^2}+\beta\Big)\eta^n+\frac{\rho_s h_s}{\Delta t^2}\eta^{n-1}\Big)v_3\circ\boldsymbol{x}_f^n\,d\gamma = \\
&\qquad = -\int_{\Gamma^n}\Big(\frac{\rho_s h_s}{\Delta t}+\beta\Delta t\Big)u_3^{n+1}v_3\delta^n\,d\gamma + \\
&\qquad\quad -\int_{\Gamma^n}\Big(\Big(-\frac{\rho_s h_s}{\Delta t^2}+\beta\Big)\eta^n+\frac{\rho_s h_s}{\Delta t^2}\eta^{n-1}\Big)\circ(\boldsymbol{x}_f^n)^{-1}v_3\delta^n\,d\gamma.
\end{aligned} \tag{21}$$

For the space discretization of this problem and of the harmonic extension (12) and (11), let us introduce two inf-sup compatible finite dimensional subspaces $\boldsymbol{V}_h^n\subset\boldsymbol{V}^n$ and $Q_h^n\subset Q^n$ and the finite dimensional subspaces $\boldsymbol{V}_{\boldsymbol{g},h}^n\subset\boldsymbol{V}_{\boldsymbol{g}}^n$ and $\boldsymbol{M}_h^0\subset\boldsymbol{M}^0$. Therefore, we can consider the following algorithm for the solution of the coupled problem given by (18), with $T=0$ and $\beta_2=\beta$:

Algorithm 1

`Given the quantities` $\boldsymbol{u}_h^n,\eta_h^n,\boldsymbol{x}_f^n$ `and the domain` Ω^n

1) `Solve the fluid problem on the configuration` Ω^n`: find` $\boldsymbol{u}_h^{n+1}\in\boldsymbol{V}_{\boldsymbol{g},h}^n$ `and` $p_h^{n+1}\in Q_h^n$ `such that`

$$\begin{cases}
\dfrac{1}{\Delta t}(\boldsymbol{u}_h^{n+1},\boldsymbol{v})_n + a(\boldsymbol{u}_h^{n+1},\boldsymbol{v}_h)_n + (((\boldsymbol{u}_h^n-\widetilde{\boldsymbol{w}}_h^n)\cdot\nabla)\boldsymbol{u}_h^{n+1},\boldsymbol{v}_h)_n + \\
\qquad +\displaystyle\int_{\Gamma^n}\Big(\frac{\rho_s h_s}{\Delta t}+\beta\Delta t\Big)u_{3,h}^{n+1}v_{3,h}\delta^n\,d\gamma - (p_h^{n+1},\nabla\cdot\boldsymbol{v}_h)_n = \\
\qquad\quad = \dfrac{1}{\Delta t}(\boldsymbol{u}_h^n,\boldsymbol{v}_h)_n + \displaystyle\int_{\Gamma_N^n}\boldsymbol{h}\cdot\boldsymbol{v}\,d\gamma + \\
\qquad\quad -\displaystyle\int_{\Gamma^n}\Big(\Big(-\frac{\rho_s h_s}{\Delta t^2}+\beta\eta_h^n\Big)+\frac{\rho_s h_s}{\Delta t^2}\eta^{n-1}\Big)\circ(\boldsymbol{x}_f^n)^{-1}v_{3,h}\delta^n\,d\gamma \\
(q_h,\nabla\cdot\boldsymbol{u}_h^{n+1})_n = 0
\end{cases} \tag{22}$$

`for all` $\boldsymbol{v}_h\in\boldsymbol{V}_h^n$ `and` $q_h\in Q_h^n$.

2) `Compute the structure displacement from` (20)

$$\eta_h^{n+1} = \Delta t(u_{3,h}^{n+1}\circ x_f^n)|_{\Gamma^0} + \eta_h^n.$$

3) `Solve the harmonic extension operator: find` $\boldsymbol{w}_h^{n+1}\in\boldsymbol{M}_h^0$ `such that`

$$\begin{cases}
(\nabla\boldsymbol{w}_h^{n+1},\nabla\boldsymbol{\psi}_h)_0 = 0 \\
\boldsymbol{w}_h^{n+1}|_{\Gamma^0} = (\boldsymbol{u}_h^{n+1}\circ\boldsymbol{x}_f^n)|_{\Gamma^0}
\end{cases}$$

`for all` $\boldsymbol{\psi}_h\in\boldsymbol{M}_h^0$.

4) `Move the points of the fluid domain`

$$\boldsymbol{x}_f^{n+1}(\boldsymbol{x}_0) = \boldsymbol{x}_f^n(\boldsymbol{x}_0) + \Delta t\, \boldsymbol{w}_h^{n+1}, \quad \forall \boldsymbol{x}^0 \in \Omega^0.$$

We point out that, thanks to (21), we do not need to solve the structure equation anymore, since it is embedded in the fluid problem. The latter is actually a problem with Robin boundary conditions for the normal component of the velocity on Γ^n, namely:

$$\Big(\sigma_3^{n+1} + \delta^n\Big(\frac{\rho_s h_s}{\Delta t} + \beta\Delta t\Big)u_3^{n+1}\Big)\Big|_{\Gamma^n} =$$

$$= -\Big(\Big(-\frac{\rho_s h_s}{\Delta t^2} + \beta\Big)\eta^n + \frac{\rho_s h_s}{\Delta t^2}\eta^{n-1}\Big) \circ (x_f^n)^{-1}\delta^n. \tag{23}$$

This condition allows one to couple in an implicit way the interface conditions (13) by solving only a fluid problem, i.e. without subiterating. This can be obtained, for example, resorting to an available standard fluid solver. Therefore, since we are treating in an explicit way the movement of the fluid domain, with this algorithm we have to solve only one fluid problem and one harmonic extension equation at each time step.

4.1.2 Pre-stressed model

Let us consider all the terms in (16). We introduce the notation

$$C = \nabla_{\boldsymbol{\xi}}\boldsymbol{\phi} = [\boldsymbol{a}_1, \boldsymbol{a}_2] \in \mathbb{R}^{3\times 2}, \quad F^n = \nabla_{\boldsymbol{x}_0}\boldsymbol{x}_f^n \in \mathbb{R}^{3\times 3}$$

where $\boldsymbol{\phi}$ is the mapping defining the reference membrane surface Γ^0 (see Section 2.1). The pre-stress tensor in the reference configuration Γ^0 expressed in Cartesian coordinate is then given by

$$\widetilde{T} = CTC^T \in \mathbb{R}^{3\times 3}.$$

We point out that $\widetilde{T}$ can be computed starting from the reference configuration Γ^0. In this case, equation (21) becomes:

$$\begin{aligned}
&\frac{1}{\Delta t}(\boldsymbol{u}^{n+1}, \boldsymbol{v})_n - \frac{1}{\Delta t}(\boldsymbol{u}^n, \boldsymbol{v})_n + a(\boldsymbol{u}^{n+1}, \boldsymbol{v})_n + \\
&\quad + (((\boldsymbol{u}^n - \widetilde{\boldsymbol{w}}^n)\cdot\nabla)\boldsymbol{u}^{n+1}, \boldsymbol{v})_n - (p^{n+1}, \nabla\cdot\boldsymbol{v})_n + \\
&\quad - \int_{\Gamma^n}\Big(\Big(\frac{\rho_s h_s}{\Delta t} + \beta_2\Delta t\Big)u_3^{n+1}v_3 + \Delta t\, F^n\,\widetilde{T}\,(F^n)^T\,\nabla u_3^{n+1}\cdot\nabla v_3\Big)\delta^n\, d\gamma + \\
&\quad - \int_{\Gamma^n}\Big(\Big(-\frac{\rho_s h_s}{\Delta t^2} + \beta_2\Big)\eta^n + \frac{\rho_s h_s}{\Delta t^2}\eta^{n-1}\Big)\circ(\boldsymbol{x}_f^n)^{-1}v_3\delta^n\, d\gamma + \\
&\quad - \int_{\Gamma^n} F^n\,\widetilde{T}\,(F^n)^T\,\nabla(\eta^n\circ(\boldsymbol{x}_f^n)^{-1})\cdot\nabla v_3\delta^n\, d\gamma.
\end{aligned}$$

The operator ∇ in the previous equation has to be understood as a derivation with respect to the current coordinate $\boldsymbol{x}_f$. We point out that in this case we

do not recover a Robin boundary condition at the interface, since it is necessary to build also a differential operator on this part of boundary. In particular, we have the following boundary condition

$$\Big(\sigma_3^{n+1} + \Big(\delta^n\Big(\frac{\rho_s h_s}{\Delta t} + \beta_2 \Delta t\Big) u_3^{n+1} + \Delta t \nabla \cdot (\delta^n F^n \widetilde{T}(F^n)^T \nabla u_3^{n+1})\Big)\delta^n\Big)\Big|_{\Gamma^n} =$$

$$= -\Big(\delta^n\Big(-\frac{\rho_s h_s}{\Delta t^2} + \beta_2\Big)\eta^n + \delta^n \frac{\rho_s h_s}{\Delta t^2}\eta^{n-1} + \nabla \cdot (\delta^n F^n \widetilde{T}(F^n)^T \nabla \eta^n)\Big) \circ (\boldsymbol{x}_f^n)^{-1}. \tag{24}$$

We refer to condition (24) as *generalized Robin* condition.

4.2 Implicit treatment of the interface position (Implicit Robin scheme)

If we want to treat in an implicit way also the interface position, we can think to embed Algorithm 1 in an iterative cycle, in which the fluid domain is updated at each subiteration until convergence. We detail the case of an algebraic model for the structure and for the sake of clarity we omit the index h, corresponding to space discretization:

Algorithm 2

`Given the quantities` $\boldsymbol{u}^n, \eta^n, \boldsymbol{x}_f^n$ `and the domain` Ω^n `and posing` $\boldsymbol{u}_0^{n+1} = \boldsymbol{u}^n, \boldsymbol{x}_{f,0}^{n+1} = \boldsymbol{x}_f^n$ `and` $\Omega_0^{n+1} = \Omega^n$, `do until convergence`

1) `Solve the fluid problem with Robin boundary condition at the interface on the configuration` Ω_k^{n+1}: `find` $\boldsymbol{u}_{k+1}^{n+1} \in \boldsymbol{V}_{\boldsymbol{g},k}^{n+1}$ `and` $p_{k+1}^{n+1} \in Q_k^{n+1}$ `such that`

$$\begin{cases} \dfrac{1}{\Delta t}(\boldsymbol{u}_{k+1}^{n+1}, \boldsymbol{v})_{n+1,k} + a(\boldsymbol{u}_{k+1}^{n+1}, \boldsymbol{v})_{n+1,k} + \\ \quad +(((\boldsymbol{u}_k^{n+1} - \widetilde{\boldsymbol{w}}_k^{n+1}) \cdot \nabla)\boldsymbol{u}_{k+1}^{n+1}, \boldsymbol{v})_{n+1,k} + \\ \quad + \displaystyle\int_{\Gamma_k^{n+1}} \beta \Delta t u_{3,k+1}^{n+1} v_3 \delta_k^{n+1}\, d\gamma - (p_{k+1}^{n+1}, \nabla \cdot \boldsymbol{v}_h)_{n+1,k} = \\ \quad = \dfrac{1}{\Delta t}(\boldsymbol{u}^n, \boldsymbol{v})_{n+1,k} + \displaystyle\int_{\Gamma_{N,k}^{n+1}} \boldsymbol{h} \cdot \boldsymbol{v}\, d\gamma - \int_{\Gamma_k^{n+1}} \beta \eta^n \circ (\boldsymbol{x}_{f,k}^{n+1})^{-1} v_3 \delta_k^{n+1}\, d\gamma \\ (q, \nabla \cdot \boldsymbol{u}_{k+1}^{n+1})_{n+1,k} = 0 \end{cases}$$

`for all` $\boldsymbol{v} \in \boldsymbol{V}_k^{n+1}$ `and` $q \in Q_k^{n+1}$.

2) `Compute the structure displacement`

$$\eta_{k+1}^{n+1} = \Delta t (u_{3,k+1}^{n+1} \circ \boldsymbol{x}_{f,k}^{n+1})|_{\Gamma^0} + \eta^n.$$

3) `Solve the harmonic extension operator: find` $\boldsymbol{w}_{k+1}^{n+1} \in \boldsymbol{M}^0$ `such that`

$$\begin{cases} (\nabla \boldsymbol{w}_{k+1}^{n+1}, \nabla \boldsymbol{\psi})_0 = 0 \\ \boldsymbol{w}_{k+1}^{n+1}|_{\Gamma^0} = (\boldsymbol{u}_{k+1}^{n+1} \circ \boldsymbol{x}_{f,k}^{n+1})|_{\Gamma^0} \end{cases}$$

`for all` $\boldsymbol{\psi} \in \boldsymbol{M}^0$.

4) `Move the points of the fluid domain`

$$\boldsymbol{x}_{f,k+1}^{n+1}(\boldsymbol{x}_0) = \boldsymbol{x}_f^n(\boldsymbol{x}_0) + \Delta t\, \boldsymbol{w}_{k+1}^{n+1}, \quad \forall \boldsymbol{x}^0 \in \Omega^0.$$

5) `Check the stopping criterion`

$$\max\left\{ \frac{\|\eta_{k+1}^{n+1} - \eta_k^{n+1}\|_{L^2(\Gamma^0)}}{\|\eta_{k+1}^{n+1}\|_{L^2(\Gamma^0)}}; \frac{\|\boldsymbol{u}_{k+1}^{n+1} - \boldsymbol{u}_k^{n+1}\|_{L^2(\Omega_k^{n+1})}}{\|\boldsymbol{u}_{k+1}^{n+1}\|_{L^2(\Omega_k^{n+1})}}; \frac{\|p_{k+1}^{n+1} - p_k^{n+1}\|_{L^2(\Omega_k^{n+1})}}{\|p_{k+1}^{n+1}\|_{L^2(\Omega_k^{n+1})}} \right\} < \varepsilon. \tag{25}$$

`If satisfied, then exit.`

We have indicated with $(\cdot,\cdot)_{m,l}$ the $L^2(\Omega_l^m)$ inner product. We point out that, at convergence, the convective term is also treated in an implicit way. Obviously, Algorithm 2, as well as Algorithm 1, can be easily extended to the inertial-algebraic and pre-stressed structure models.

4.3 Stability analysis of the Robin schemes

In this section, we want to derive an *a priori* estimate for the algorithms proposed in the previous sections. To simplify the presentation, we consider only the space-continuous case. Yet the extension of the results to the fully discrete problem is straightforward. We limit our analysis to the homogeneous case, $\boldsymbol{g} = \boldsymbol{0}$ and $\boldsymbol{h} = \boldsymbol{0}$, and to the algebraic model case. Moreover, for the sake of simplicity, we refer to a divergence-free subspace of $\boldsymbol{V}^{n+1}$. We recall the following identity (*geometrical conservation law* (GCL), see [16, 17]):

$$\int_{\Omega^n} \boldsymbol{\psi}_i \boldsymbol{\psi}_j \, d\omega - \int_{\Omega^{n-1}} \boldsymbol{\psi}_i \boldsymbol{\psi}_j \, d\omega = I_{t^{n-1}}^{t^n} \Big[\int_{\Omega^t} \boldsymbol{\psi}_i \boldsymbol{\psi}_j \nabla \cdot \widetilde{\boldsymbol{w}} \, d\omega \Big], \tag{26}$$

where $\boldsymbol{\psi}_k$ is the generic finite element basis function and $I_{t^{n-1}}^{t^n}$ is a time integration quadrature formula whose degree of exactness is $d \cdot s - 1$, where d is the dimension of the fluid domain and s is the degree of the polynomial used to represent the time evolution of the nodal displacement. For example, in our case $d = 3$ and if we choose a linear time variation of the nodal displacement in each time slab ($s = 1$), in order to satisfy (26) it is sufficient to use a two point Gauss quadrature formula, obtaining

$$\int_{\Omega^n} \boldsymbol{\psi}_i \boldsymbol{\psi}_j \, d\omega - \int_{\Omega^{n-1}} \boldsymbol{\psi}_i \boldsymbol{\psi}_j \, d\omega = \frac{\Delta t}{2} \sum_{i=\pm \Delta t\sqrt{3}/4} \int_{\Omega^{n-1/2+i}} \boldsymbol{\psi}_i \boldsymbol{\psi}_j \nabla \cdot \widetilde{\boldsymbol{w}}^{n-1/2+i} \, d\omega.$$

In the particular case of cylindrical configuration and radial displacement, it can be shown (see [16]) that a midpoint rule is sufficient to satisfy (26), namely:

$$\int_{\Omega^n} \boldsymbol{\psi}_i \boldsymbol{\psi}_j \, d\omega - \int_{\Omega^{n-1}} \boldsymbol{\psi}_i \boldsymbol{\psi}_j \, d\omega = \Delta t \int_{\Omega^{n-1/2}} \boldsymbol{\psi}_i \boldsymbol{\psi}_j \nabla \cdot \widetilde{\boldsymbol{w}}^{n-1/2} \, d\omega. \tag{27}$$

Hereafter, we detail the case of cylindrical geometry where a mid-point rule can be employed. The result generalizes immediately to a more complex geometry when adopting the proper quadrature formula so as to satisfy the GCL. Let us consider the *conservative* formulation of problem (21) (with $\rho_s = 0$), that becomes (see [16, 17]):

$$\begin{aligned} \frac{1}{\Delta t}(\boldsymbol{u}^n, \boldsymbol{v})_m - \frac{1}{\Delta t}(\boldsymbol{u}^{n-1}, \boldsymbol{v})_{m-1} + a(\boldsymbol{u}^n, \boldsymbol{v})_{m-1/2} + \\ +(((\boldsymbol{u}^m - \widetilde{\boldsymbol{w}}^m) \cdot \nabla)\boldsymbol{u}^n, \boldsymbol{v})_{m-1/2} - (\nabla \cdot \widetilde{\boldsymbol{w}}^m \boldsymbol{u}^n, \boldsymbol{v})_{m-1/2} + \\ + \int_{\Gamma^{m-1/2}} \beta(\Delta t u_3^n + \eta^{n-1} \circ (\boldsymbol{x}_f^{m-1/2})^{-1}) v_3 \delta^{m-1/2} \, d\gamma = 0 \end{aligned} \tag{28}$$

where $m = n$ for the implicit Robin scheme and $m = n - 1$ for the explicit Robin scheme. We point out that, since we consider a linear time variation of the nodes displacement, the domain velocity $\widetilde{\boldsymbol{w}}^m$ is constant in the time slab $[t^{m-1}, t^m]$ and, in particular, we have $\widetilde{\boldsymbol{w}}^m = \widetilde{\boldsymbol{w}}^{m-1/2}$.

Let us indicate with $\|\cdot\|_n$ the $L^2(\Omega^n)$ norm and with $\|\cdot\|_{\Gamma_0}$ the $L^2(\Gamma^0)$ norm. The following result holds true

Theorem 1 *Setting $N = T/\Delta t$, if*

$$(\boldsymbol{u}^m \cdot \widetilde{\boldsymbol{a}}_3)|_{\Gamma_N^{m-1/2}} \geq 0, \tag{29}$$

the following a priori estimate for problem given by (28) and (20) in the homogeneous case, $\boldsymbol{g} = \boldsymbol{0}$ and $\boldsymbol{h} = \boldsymbol{0}$, holds:

$$\|\boldsymbol{u}^N\|_M^2 + 2\mu C_k \Delta t \sum_{k=M-N+1}^{M} \|\nabla \boldsymbol{u}^k\|_{k-1/2}^2 + \beta \|\eta^N\|_{\Gamma^0}^2 \leq \|\boldsymbol{u}^0\|_0^2 + \beta \|\eta^0\|_{\Gamma^0}^2, \tag{30}$$

with $M = N - 1$ for the explicit Robin algorithm and $M = N$ for the implicit Robin one and where we pose $\Omega^{-1/2} = \Omega^0$.

Proof. Taking $\boldsymbol{v} = \boldsymbol{u}^n$ in (28), we obtain:

$$\begin{aligned} \frac{1}{\Delta t}\|\boldsymbol{u}^n\|_m^2 + \mu C_k \|\nabla \boldsymbol{u}^n\|_{m-1/2}^2 - \frac{1}{2}(\nabla \cdot (\boldsymbol{u}^m - \widetilde{\boldsymbol{w}}^m), |\boldsymbol{u}^n|^2)_{m-1/2} + \\ +\frac{1}{2}\int_{\partial\Omega^{m-1/2}} (\boldsymbol{u}^m - \widetilde{\boldsymbol{w}}^m) \cdot \widetilde{\boldsymbol{a}}_3 |\boldsymbol{u}^n|^2 d\gamma - (\nabla \cdot \widetilde{\boldsymbol{w}}^m, |\boldsymbol{u}^n|^2)_{m-1/2} + \\ + \int_{\Gamma^{m-1/2}} \beta(\Delta t u_3^n + \eta^{n-1} \circ (\boldsymbol{x}_f^{m-1/2})^{-1}) u_3^n \delta^{m-1/2} \, d\gamma \leq \frac{1}{\Delta t}(\boldsymbol{u}^{n-1}, \boldsymbol{u}^n)_{m-1} \end{aligned} \tag{31}$$

where C_k is the Korn's inequality constant. Recalling (27), the right hand side can be bounded:

$$(\boldsymbol{u}^{n-1}, \boldsymbol{u}^n)_{m-1} \leq \frac{1}{2}\|\boldsymbol{u}^n\|^2_{m-1} + \frac{1}{2}\|\boldsymbol{u}^{n-1}\|^2_{m-1} =$$

$$= \frac{1}{2}\|\boldsymbol{u}^n\|^2_{m} + \frac{1}{2}\|\boldsymbol{u}^{n-1}\|^2_{m-1} - \frac{\Delta t}{2}(\nabla \cdot \widetilde{\boldsymbol{w}}^m, |\boldsymbol{u}^n|^2)_{m-1/2}$$

and (31) becomes

$$\frac{1}{2\Delta t}\|\boldsymbol{u}^n\|^2_m + \mu C_k \|\nabla \boldsymbol{u}^n\|^2_{m-1/2} - \frac{1}{2}(\nabla \cdot (\boldsymbol{u}^m - \widetilde{\boldsymbol{w}}^m), |\boldsymbol{u}^n|^2)_{m-1/2} +$$

$$+\frac{1}{2}\int_{\partial\Omega^{m-1/2}} (\boldsymbol{u}^m - \widetilde{\boldsymbol{w}}^m)\cdot \widetilde{\boldsymbol{a}}_3 |\boldsymbol{u}^n|^2 \, d\boldsymbol{\gamma} - (\nabla \cdot \widetilde{\boldsymbol{w}}^m, |\boldsymbol{u}^n|^2)_{m-1/2} +$$

$$+\int_{\Gamma^{m-1/2}} \beta(\Delta t u_3^n + \eta^{n-1} \circ (\boldsymbol{x}_f^{m-1/2})^{-1}) u_3^n \delta^{m-1/2} \, d\gamma \leq$$

$$\leq \frac{1}{2\Delta t}\|\boldsymbol{u}^{n-1}\|^2_{m-1} - \frac{1}{2}(\nabla \cdot \widetilde{\boldsymbol{w}}^m, |\boldsymbol{u}^n|^2)_{m-1/2}.$$

Recalling that

$$\begin{cases} \nabla \cdot \boldsymbol{u}^m = 0, & \boldsymbol{u}^m|_{\Gamma_D^{m-1/2}} = \boldsymbol{0}, \\ (\widetilde{\boldsymbol{w}}^m \cdot \widetilde{\boldsymbol{a}}_3)_{\Gamma_N^{m-1/2} \cup \Gamma_D^{m-1/2}} = 0, & \widetilde{\boldsymbol{w}}^m|_{\Gamma^m} = \boldsymbol{u}^m|_{\Gamma^m} \end{cases}$$

and using (20), we obtain:

$$\frac{1}{2\Delta t}\|\boldsymbol{u}^n\|^2_m + \mu C_k \|\nabla \boldsymbol{u}^n\|^2_{m-1/2} + \frac{1}{2}\int_{\Gamma_N^{m-1/2}} \boldsymbol{u}^m \cdot \widetilde{\boldsymbol{a}}_3 |\boldsymbol{u}^n|^2 \, d\boldsymbol{\gamma} +$$

$$+ \int_{\Gamma^0} \beta \eta^n \frac{(\eta^n - \eta^{n-1})}{\Delta t} d\gamma \leq \frac{1}{2\Delta t}\|\boldsymbol{u}^{n-1}\|^2_{m-1}. \tag{32}$$

If we assume that hypothesis (29) holds, we obtain

$$\int_{\Gamma_N^{m-1/2}} \boldsymbol{u}^m \cdot \widetilde{\boldsymbol{a}}_3 |\boldsymbol{u}^n|^2 \, d\boldsymbol{\gamma} \geq 0.$$

Therefore, from (32) we obtain

$$\|\boldsymbol{u}^n\|^2_m + 2\mu C_k \Delta t \|\nabla \boldsymbol{u}^n\|^2_{m-1/2} + \beta \|\eta^n\|^2_{\Gamma^0} \leq \|\boldsymbol{u}^{n-1}\|^2_{m-1} + \beta \|\eta^{n-1}\|^2_{\Gamma^0}.$$

Summing up over the index n, we obtain the final estimate (30). □

We point out that assumption (29) is verified in many applications, for example in haemodynamics, where the heart pumps the blood only in the downstream direction (see [46]).

5 Flow rate boundary conditions

In many engineering fluid dynamic problems, some portions of the computational domain's boundary do not correspond to any physical boundary and are just introduced to limit the domain of interest (see Figure 3). The prescription of boundary conditions on such *artificial* boundaries can be source of inaccuracies. In particular, in several contexts of internal fluid dynamics there is sometimes the

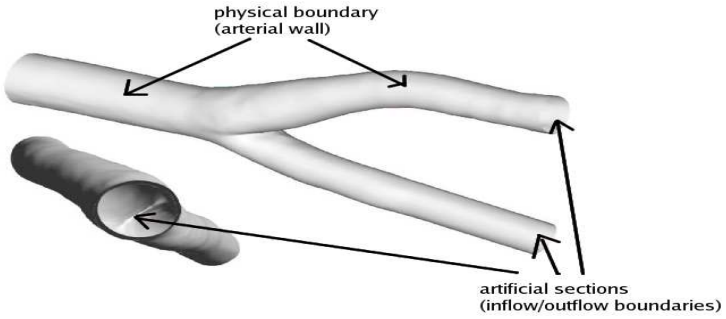

Figure 3: Example of truncated computational domain: carotid bifurcation (cast by D. Liepsch - FH Munich)

.

need to deal with *defective boundary data sets*, namely data that are not enough to have a mathematically well posed problem. For example, in haemodynamics it is often the case that only the flow rate

$$\int_{\Sigma} \boldsymbol{u} \cdot \widetilde{\boldsymbol{a}}_3 \, d\sigma = F \tag{33}$$

is available from clinical measurements as boundary condition over an artificial section Σ. This condition also appears in the geometrical multiscale modelization of the cardiovascular system (see [13, 45, 43]), where a 3D model is coupled with a reduced one, receiving from it only defective data as boundary conditions at the interface. The problem arising by imposing condition (33) is not well posed, since it prescribes only an average information over all the boundary Σ. The flow rate problem, i.e. the imposition of only condition (33) over the whole section Σ, has been extensively analyzed for the rigid case in [28, 14, 47, 48, 49, 21]. In particular, in [14, 47, 48, 49] a flow rate boundary condition is treated as a constraint, imposed by a Lagrange multiplier (*augmented formulation*). Here, we want to extend this approach to the compliant case, in combination with the Robin scheme. Referring to Figure 2 (right), we want to prescribe the flow rates F_i at the artificial sections $\Gamma_i^t, i = 1, \ldots, m$. Therefore, setting $\widetilde{\boldsymbol{V}}^t = \{\boldsymbol{v} \in \boldsymbol{H}^1(\Omega^t) : (\boldsymbol{v} \cdot \widetilde{\boldsymbol{a}}_\alpha)|_{\Gamma^t} = 0\}$, the weak formulation (15) is replaced, for each time

t, by the following augmented one (see [47])

$$\begin{cases} \left(\dfrac{D^A \boldsymbol{u}}{Dt}, \boldsymbol{v}\right) + a(\boldsymbol{u}, \boldsymbol{v}) + (((\boldsymbol{u} - \widetilde{\boldsymbol{w}}) \cdot \nabla)\boldsymbol{u}, \boldsymbol{v}) - (p, \nabla \cdot \boldsymbol{v}) + \\ \qquad + \displaystyle\sum_{i=1}^{m} \lambda_i \int_{\Gamma_i^t} \boldsymbol{v} \cdot \widetilde{\boldsymbol{a}}_3 \, d\gamma = \int_{\Gamma^t} \sigma_3 v_3 \, d\gamma \\ (q, \nabla \cdot \boldsymbol{u}) = 0 \\ \boldsymbol{u}|_{t=0} = \boldsymbol{u}_0 \\ \displaystyle\int_{\Gamma_i^t} \boldsymbol{u} \cdot \widetilde{\boldsymbol{a}}_3 \, d\gamma = F_i(t), \quad i = 1, \ldots, m \end{cases}$$

for all $\boldsymbol{v} \in \widetilde{\boldsymbol{V}}^t$ and $q \in Q^t$ and where $F_i(t)$, $i = 1, \ldots, m$ are given continuous functions and $\lambda_i(t) \in L^2(0, T)$, $i = 1, \ldots, m$ are the (unknown) Lagrange multipliers.

For the sake of simplicity, in the sequel let us consider an algebraic model for the structure and the explicit Robin scheme. Therefore, it is sufficient to replace problem (22) at step 1) in Algorithm 1 with the following augmented formulation: find $\boldsymbol{u}^{n+1} \in \widetilde{\boldsymbol{V}}^n$ and $q^{n+1} \in Q^n$, such that

$$\begin{cases} \dfrac{1}{\Delta t}(\boldsymbol{u}^{n+1}, \boldsymbol{v})_n + a(\boldsymbol{u}^{n+1}, \boldsymbol{v})_n + (((\boldsymbol{u}^n - \widetilde{\boldsymbol{w}}^n) \cdot \nabla)\boldsymbol{u}^{n+1}, \boldsymbol{v})_n - (p^{n+1}, \nabla \cdot \boldsymbol{v})_n + \\ \qquad + \displaystyle\int_{\Gamma^n} \beta \Delta t u_3^{n+1} v_3 \delta^n \, d\gamma + \sum_{i=1}^{m} \lambda_i^{n+1} \int_{\Gamma_i^n} \boldsymbol{v} \cdot \widetilde{\boldsymbol{a}}_3 \, d\gamma = \\ \qquad = \dfrac{1}{\Delta t}(\boldsymbol{u}^n, \boldsymbol{v})_n - \displaystyle\int_{\Gamma^n} \beta \eta^n \circ (x_f^n)^{-1} v_3 \delta^n \, d\gamma \\ (q, \nabla \cdot \boldsymbol{u}^{n+1})_n = 0 \\ \displaystyle\int_{\Gamma_i^n} \boldsymbol{u}^{n+1} \cdot \widetilde{\boldsymbol{a}}_3 \, d\gamma = F_i^{n+1}, \quad i = 1, \ldots, m \end{cases} \tag{34}$$

for all $\boldsymbol{v} \in \widetilde{\boldsymbol{V}}^n$ and $q \in Q^n$, where we set $F_i^n = F_i(t^n)$, $i = 1, \ldots, m$. For the numerical solution of problem (34), we can use one of the algorithms proposed in [47, 48, 49].

Remark 2 *Due to the mass conservation law, in the rigid case is not possible to prescribe an arbitrary flow rate on all the artificial section. For example, at the section Γ_1^t, the flow rate $F_1(t)$ has to satisfy $F_1(t) = -\sum_{j=2}^m F_j(t)$, for compatibility with the mass conservation equation. In the compliant case instead, this compatibility condition does not hold anymore and it is possible to prescribe the flow rate on all the artificial sections. In this case, the mass conservation law reads:*

$$\sum_{i=1}^{m} \int_{\Gamma_i^t} \boldsymbol{u} \cdot \widetilde{\boldsymbol{a}}_3 \, d\gamma + \int_{\Gamma^t} \frac{\partial \eta}{\partial t} \circ \boldsymbol{x}_f^{-1} \, d\gamma = 0.$$

Nevertheless, if we use an iterative fluid/structure algorithm to solve the fluid-structure coupled problem in which the structure prescribes a Dirichlet datum at the interface to the fluid (as, e.g., in the Dirichlet-Neumann algorithm, see for example [39, 7]), an incompatibility might arise again between the flow rates F_i, $i = 1, \dots, m$ and the velocity at the interface, if

$$\int_{\Gamma^t} \Big(\frac{\partial \eta}{\partial t} \circ x_f^{-1} \Big) d\gamma \neq - \sum_{i=1}^{m} F_i(t).$$

This problem can be overcome by forcing that the mass conservation law is satisfied through the introduction of a Lagrange multiplier also for the displacement of the interface, as suggested in [26, 39]. However, when adopting the Robin method, this problem is completely overcome and no difficulties are encountered in imposing the flow rate on all the artificial sections. This is a clear advantage of the Robin scheme with respect to Dirichlet-Neumann strategy.

6 Absorbing boundary conditions

It is well known that, even if the fluid motion is described by parabolic equations, the nature of the fluid-structure interaction problem in haemodynamics presents some features of hyperbolic type. In particular, pressure waves travel along the fluid domain (see [40, 4, 18, 13]). The imposition of a suitable outflow boundary condition, which does not induce spurious reflections, is a major issue in this kind of problems. In order to avoid the phenomenon of spurious reflections, it is possible to prescribe a suitable *absorbing* boundary condition, by coupling the 3D compliant model with a 1D reduced model, as proposed in [13] (geometrical multiscale approach). In particular, referring to the compliant cylinder in Figure

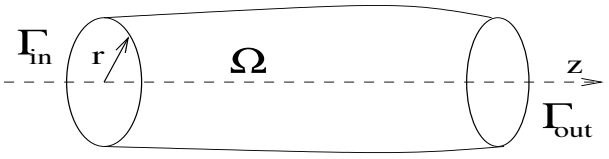

Figure 4: Reference cylinder Ω

4, whose length is L, a simplified 1D model can be obtained integrating at each time t the Navier-Stokes equations over each section S normal to the axis z of the cylinder. The 1D model reads, for each $t > 0$ and $0 < z < L$, (see [13, 18, 20]):

$$\begin{cases} \dfrac{\partial A}{\partial t} + \dfrac{\partial F}{\partial z} = 0 \\ \dfrac{\partial F}{\partial t} + \dfrac{\partial}{\partial z}\Big(\alpha \dfrac{F^2}{A}\Big) + A \dfrac{\partial P}{\partial z} + K_R \dfrac{F}{A} = 0 \end{cases} \tag{35}$$

where F is the flow rate through S, A is the area of S, P the mean pressure over S, K_R is a resistance parameter which accounts for the fluid viscosity,

while α accounts for the shape of the velocity profile over S. For example, the choice $\alpha = 1$ corresponds to a flat velocity profile. System (35) is a system of two equations in three unknowns (P, F, A). For its closure, a third equation is provided by a suitable wall model relating the radial displacement (and therefore the area A) to the mean pressure P. In particular, considering the pure algebraic model given by (1), with $\rho_s = 0$, we obtain

$$P = \frac{\beta}{\pi}(\sqrt{A} - \sqrt{A^0}) \tag{36}$$

where A^0 is the area of the surface S at $t = 0$, the parameter β is given by (8) and we approximate the normal stress with the pressure. Then, system (35) turns out to be hyperbolic and it allows to capture propagative phenomena along the axis of the cylinder. It possesses two distinct eigenvalues and the corresponding eigenfunctions are the characteristic variables, given by (see [39, 13])

$$W_{1,2} = \frac{F}{A} \pm \frac{2}{\sqrt{\rho_s}}(\sqrt{P + \beta\sqrt{A_0}} - \sqrt{\beta\sqrt{A_0}}).$$

Here, we propose to derive an absorbing outflow boundary condition without coupling the 3D model with the reduced one, but simply by imposing that the characteristic variable entering in the 3D computational domain is zero, meaning that no information is entering. In particular, we impose

$$W_2|_{\Gamma^t_{out}} = \Big(\frac{F}{A} - \frac{2}{\sqrt{\rho_s}}(\sqrt{P + \beta\sqrt{A_0}} - \sqrt{\beta\sqrt{A_0}})\Big)\Big|_{\Gamma^t_{out}} = 0,$$

obtaining

$$P|_{\Gamma^t_{out}} = \Big(\Big(\frac{1}{2\sqrt{2}}\frac{F}{A} + \sqrt{\beta\sqrt{A^0}}\Big)^2 - \beta\sqrt{A^0}\Big)\Big|_{\Gamma^t_{out}}. \tag{37}$$

Relation (37) relate the mean pressure P to the flow rate F at the outlet. Since the latter quantity is unknown, we can treat it in an explicit way, interpreting the mean pressure boundary condition (37) as a normal stress, constant in space, as suggested in [28]. This leads to the following *absorbing Neumann boundary condition* at the outlet

$$({\sigma_f}^{n+1}\widetilde{\boldsymbol{a}}_3)|_{\Gamma^n_{out}} = \Big(\Big(\Big(\frac{1}{2\sqrt{2}}\frac{F^n}{A^n} + \sqrt{\beta\sqrt{A^0}}\Big)^2 - \beta\sqrt{A^0}\Big)\widetilde{\boldsymbol{a}}_3\Big)\Big|_{\Gamma^n_{out}}. \tag{38}$$

Obviously, in the implicit Robin Algorithm 2, we can take the flow rate F^{n+1}_k at the previous subiteration instead of F^n in (38) (and similarly for A^{n+1}_k and $\Gamma^{n+1}_{out,k}$).

Alternatively, one could treat in an explicit way the mean pressure in (37) and prescribe the following *absorbing flow rate boundary condition* at the outlet

$$\int_{\Gamma^n_{out}} \boldsymbol{u}^{n+1} \cdot \widetilde{\boldsymbol{a}}_3 \, d\gamma = F^{n+1}|_{\Gamma^n_{out}} = \Big(2\sqrt{2}A^n\Big(\sqrt{\beta\sqrt{A^0} - P^n} - \sqrt{\beta\sqrt{A^0}}\Big)\Big)\Big|_{\Gamma^n_{out}}, \tag{39}$$

which can be imposed using the flow rate approach described in Section 5.

We point out that, for a geometry like the one depicted in Fig. 2, we can assume that condition (37) holds at each outflow section, provided that we ideally extend each brunch as an infinitly long cylinder. Therefore, we can reduce the spurious reflections also in a general domain, applying conditions (38) or (39) at the outflows.

7 Numerical results

In this section we present some numerical results with the aim of testing the methodologies proposed in Sections 3, 4, 5 and 6. In particular, in Section 7.1 we test Algorithms 1 and 2, with various structure models. In Section 7.2 we compare the numerical results obtained with and without prescribing an absorbing boundary condition. Finally, in Section 7.3 we show some results concerning the compliant flow rate problem, comparing them with the solution obtained in the rigid case. All the simulations are performed in a cylindrical domain with the 2d Finite Element code *Freefem++* (see [29]) in axi-symmetric form. We use, if not otherwise specified, $\mathbb{P}_1 bubble - \mathbb{P}_1$ elements, $\Delta t = 10^{-3}\, s$, $\mu = 0.035\, cm^3/s$, $\beta = 4 \cdot 10^5\, dyne/cm$, $\rho_s = 1\, g/cm^3$, $h_s = 0.1\, cm$ and $\mu_s = 1.5 \cdot 10^4\, dyne\, cm$. These values are taken from problems in computational haemodynamics, that inspired the present work.

7.1 Robin algorithms assessment

In the simulations of this section, the computational domain is a cylinder generated by the rotation of a rectangle $6 \times 0.5\, cm$ around its axial axis, with a space grid $h = 0.05\, cm$. Moreover, we impose the following impulsive pressure gradient between the inlet and the outlet:

$$\Delta P = \begin{cases} 5 \cdot 10^3\, dyne/cm^2 & \text{for} \quad t < 0.005\, s \\ 0 & \text{for} \quad t \geq 0.005\, s. \end{cases}$$

In the first set of simulations, we aim at testing Algorithm 1 with the different structure models proposed in Section 2, namely: algebraic ($\rho_s = 0, T = 0$), inertial-algebraic ($T = 0$) and pre-stressed models. Figure 5 and Figure 6 show the pressure field and the displacement of the structure, respectively, computed in the three cases at different times.

In the second simulation, we want to compare the results obtained using Algorithm 1 and Algorithm 2, i.e. using the explicit Robin scheme and the implicit Robin scheme, respectively. In both cases we use an algebraic model for the structure and we set $\Delta t = 0.0005\, s$. For the implicit Robin scheme we use the stopping criterion (25) and we do not need to use a relaxation procedure when updating the fluid domain. For this simulation, Algorithm 2 needs 13.55 subiterations (in average) for each time step. Figure 7 shows the pressure and

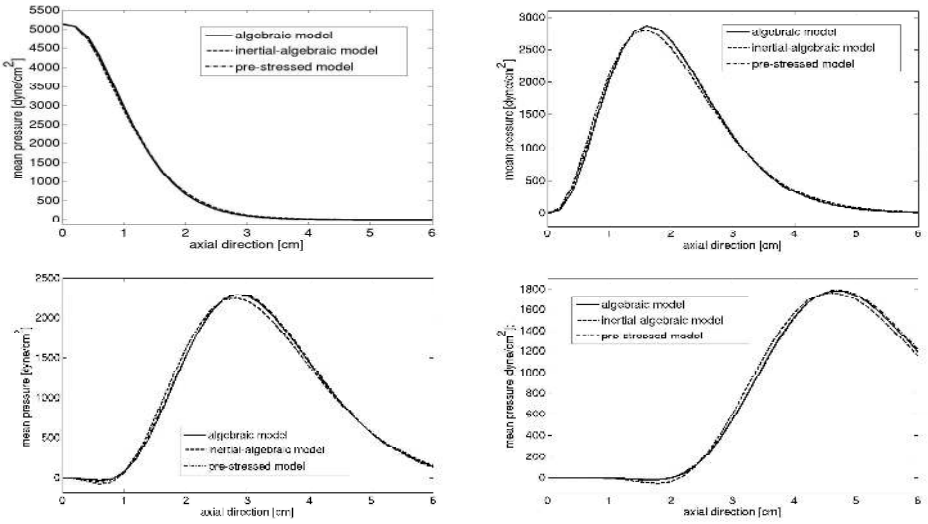

Figure 5: Mean pressure on the longitudinal sections computed with Algorithm 1 - $t = 0.004\,s$ (left, up), $t = 0.08\,s$ (right, up), $t = 0.012\,s$ (left, bottom) and $t = 0.018\,s$ (right, bottom).

the displacement of the structure obtained with the two schemes. We point out that the two results are in excellent agreement and this suggests that, in the case of a thin walled structure, the implicit treatment of the coupling conditions is essential for stability purpose, whereas the implicit treatment of the interface position does not seem to improve substantially the accuracy of the solution.

7.2 Absorbing boundary conditions

In this section we want to assess the benefit produced by the absorbing boundary conditions (38) and (39), for the same test case shown in Section 7.1, using Algorithm 1 and an algebraic model. Figure 8 compares the solutions computed with and without prescribing the absorbing condition (38). In particular, in the latter case we have imposed standard stress-free boundary conditions on the outflow section. We observe that at $t = 0.01\,s$ the wave pressure has not yet reached the end of the domain and therefore the two solutions coincides, while at $t = 0.05\,s$ the reflections have started and the two solutions differ significantly. Moreover, Figure 9 shows the mean pressure at surfaces distant $1.4\,cm$ and $3\,cm$ from the inlet, in the two cases. We notice a significant reduction of the spurious reflections by imposing condition (38). In Figure 10 (left) we compare the mean pressure obtained prescribing condition (38) in the algebraic, inertial-algebraic and pre-stressed models cases. Finally, in Fig. 10 (right) we compare the solutions obtained by using the mean pressure (38) and the flow rate (39) as absorbing boundary condition at the outlet. The latter has been prescribed with the *GMRes-based* algorithm (GS) proposed in [47]. In this plot, we have

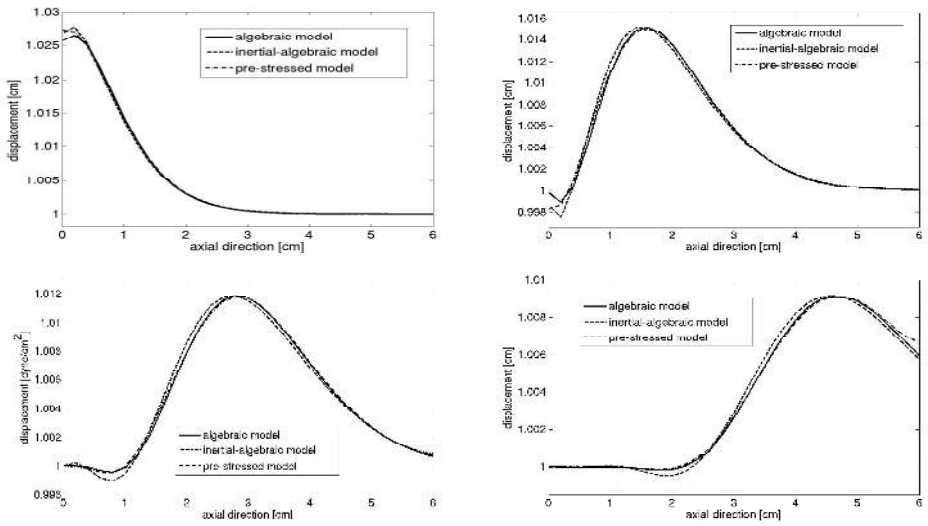

Figure 6: Displacement of the structure computed with Algorithm 1 - $t = 0.004\,s$ (left, up), $t = 0.008\,s$ (right, up), $t = 0.012\,s$ (left, bottom) and $t = 0.018\,s$ (right, bottom).

considered an algebraic model for the structure and $\Delta t = 0.002\,s$. We notice that the second approach also reduces considerably the spurious reflections, even though it is more computationally expensive than the other one (see [47]).

7.3 The Womersley solution in a compliant domain

In this section we consider a fluid-structure counterpart of a well-known solution, namely the Womersley solution, valid for a pulsatile flow in a rigid vessel (see [50]). The Womersley solution can be obtained by imposing at the inlet a sinusoidal flow rate and a free stress condition at the outlet. Such solution is of great importance in haemodynamics, since it evidences the possibility of local inversions of the axial velocity during a cardiac beat. Also, the solution corresponding to a more complex periodic wave form of the inlet flow rate can be obtained by superimposition of elementary Womersley solutions.

The goal of this section is to investigate numerically at what extent the Womersley solution is a good description of a pulsatile flow in a compliant vessel. The major difficulty is due to the fact that the duration of a cardiac beat is much longer than the "propagation" time (i.e. tha time that information takes to go from inlet to outlet). As a consequence, a bad choice of outlet boundary conditions (i.e. partially reflecting) will completely spoil the solution. To obtain a fluid-structure equivalentof the Womersley solution we consider a complaint cylindrical domain, the algebraic membrane model (1) for the artery deformation, with $\beta = 10^5\,dyne/cm$, the following flow rate boundary condition at the

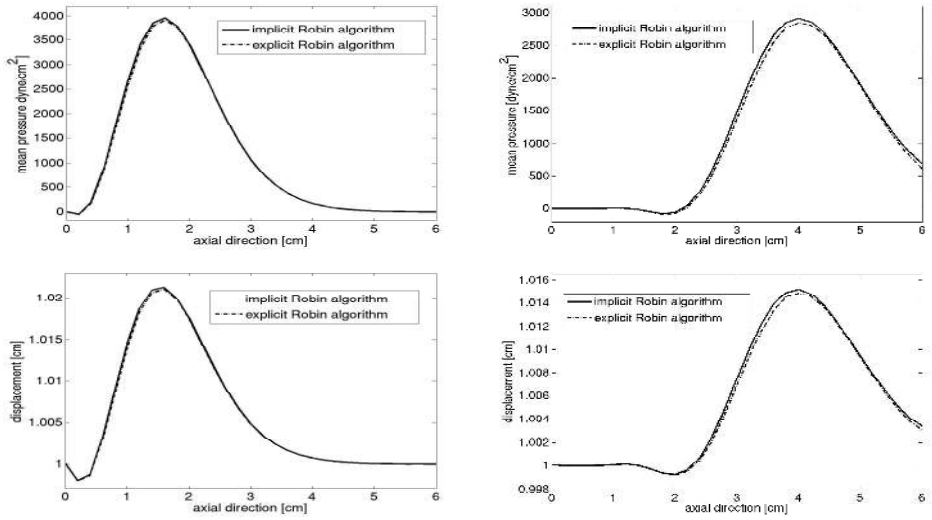

Figure 7: Mean pressure on the longitudinal sections (up) and displacement of the structure (bottom) computed with Algorithm 1 and Algorithm2 - algebraic model - $t = 0.008\,s$ (left) and $t = 0.016\,s$ (right).

inlet Γ

$$Q = 4 \cdot \sin(2\pi t)\, cm^3/s, \tag{40}$$

and the absorbing boundary condition (38) at the outlet. The computational domain is generated by the rotation of a rectangle $2.5 \times 0.5\,cm$ around its axis, with a space discretization parameter $h = 0.0025\,cm$.

Figure 12 shows the axial velocity profile on a radius at the inlet Γ, at section Γ_1 (distant $1\,cm$ from the inlet) and at section Γ_2 (distant $2\,cm$ from the inlet, see Fig. 11), for the rigid and the compliant case. Since in the compliant case the radius deforms, to be able to compare the two solutions we have recast the profile to the reference configuration. Observe that, at the inlet the two solutions are very similar, while moving into the domain, the compliant solution is delayed. This was foreseeable, since in the compliant case the propagation of the information is not immediate as in the rigid case. In particular, we have estimated a velocity of propagation $v = 222.22\,cm/s$, leading to a delay $\phi = 0.009\,s$ between sections Γ and Γ_2. This is confirmed by Figures 12 (right) where the compliant solution is also compared with the rigid solution at time $t - \phi$, showing that the Womersley solution is carried along the vessel.

We point out that we were able to achieve this comparision at a low computational cost thanks to our Robin scheme and, mostly, to the proposed absorbing boundary conditions.

This simulation shows that the Womersley profile is meaningful also in the compliant case provided we properly account for the delay due to the propagation of information at finite speed.

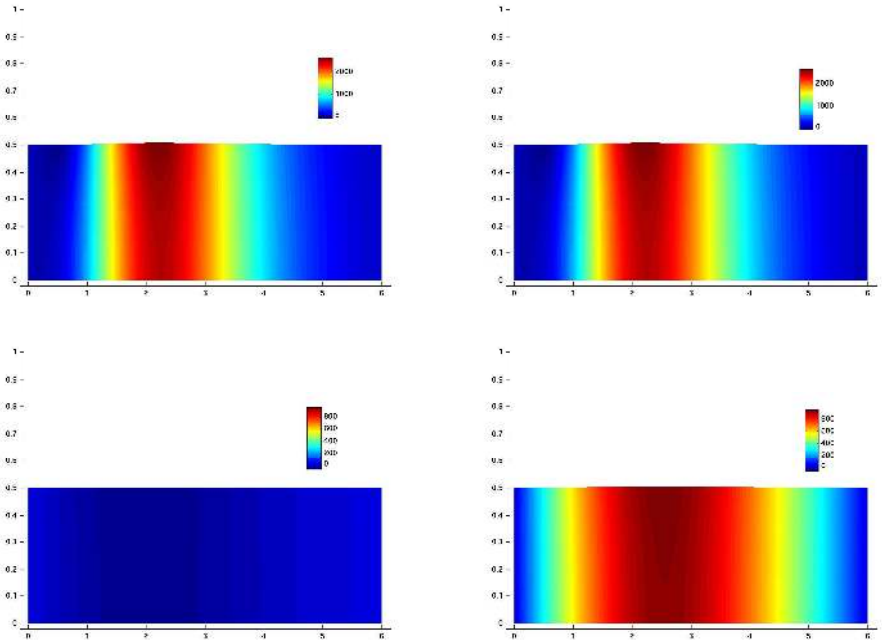

Figure 8: Pressure obtained with (left) and without (right) prescribing condition (38) - Algorithm 1 - algebraic model - $t = 0.01\,s$ (up) and $t = 0.05\,s$ (bottom).

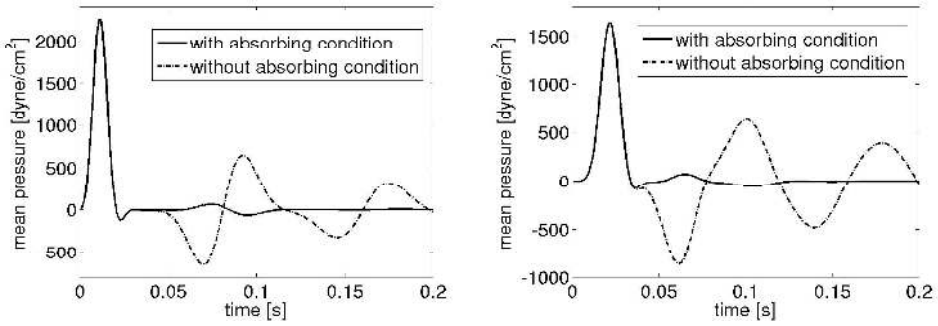

Figure 9: Mean pressure at a section distant $1.4\,cm$ (left) and $3\,cm$ (right) from the inlet - Algorithm 1 - algebraic model.

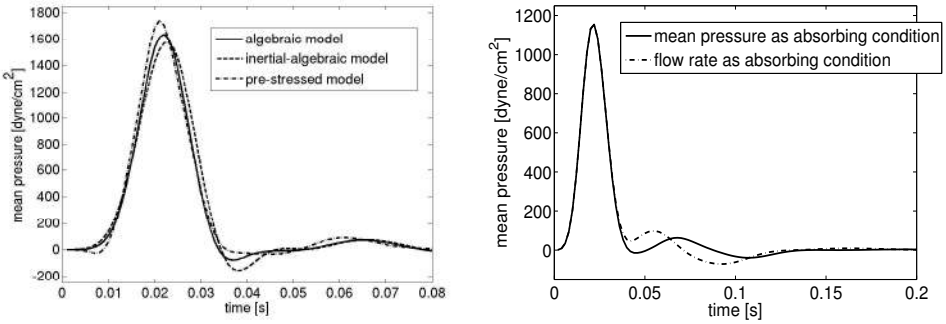

Figure 10: On the left: mean pressure at a section distant $3\,cm$ from the inlet, using the algebraic, the inertial and the generalized string model. On the right: comparison of the same quantity using the mean pressure or the flow rate as absorbing boundary condition, for the algebraic model only.

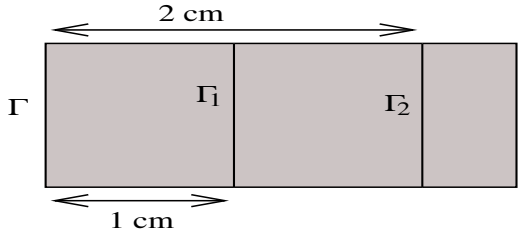

Figure 11: Computational domain

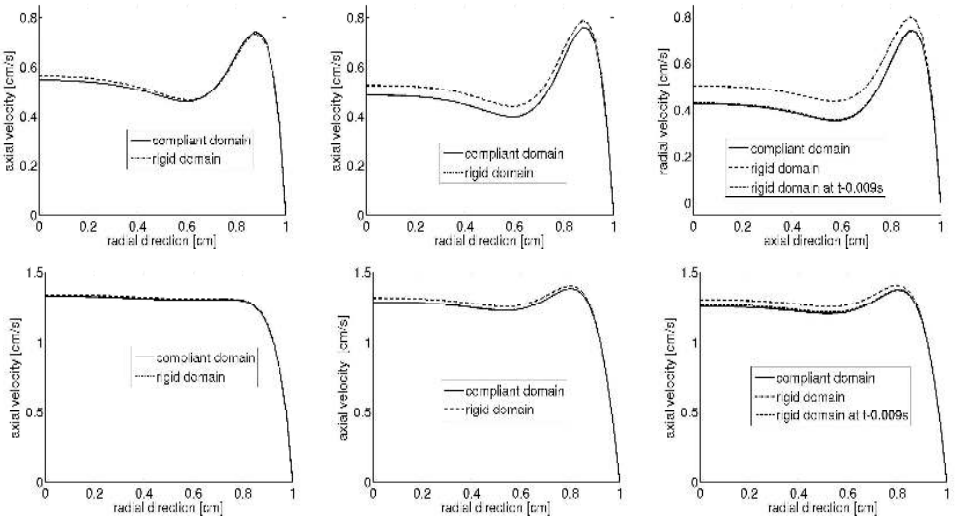

Figure 12: Axial velocity on a radius in the reference domain at the inlet Γ (left), at section Γ_1 (middle) and at section Γ_2 (right) - $t = 1.070\,s$ (up) and $t = 1.190\,s$ (down).

8 Conclusions

In this paper we have proposed a simple structure model, based on the assumption that the structure is thin, behaves like a membrane and deforms mainly in the normal direction to the mean surface. It can be written for an arbitrary surface and generalizes the independent rings and the generalized string models, introduced in literature for a cylindrical geometry. Due to its simplicity, it is very attractive for realistic applications, e.g. in haemodynamics.

Secondly, we have proposed an efficient fluid-structure coupling strategy, where the membrane model is embedded into the fluid equations resorting to generalized Robin boundary conditions. The resulting numerical scheme treats automatically in an implicit way the coupling fluid-structure conditions. On the other hand, the interface position can be treated explicitely or implicitely by fixed point iterations. In both cases, we have proven both theoretically and numerically the stability of the scheme. In particular the explicit Robin scheme is very attractive since it is stable and only requires one fluid solution per time step. On the other hand, the implicit Robin scheme seems to be competitive with other available fully implicit algorithms, since from our preliminary results, it requires a quite small number of subiterations and does not need any relaxation. However, a complete comparision in terms of computational costs is still under development.

Finally, we have proposed a new absorbing boundary condition to reduce the spurious refelctions induced by the truncation of the computational domain. These absorbing conditions are related to the geomatrical multiscale approach proposed in [13], yet avoid the coupling with the reduced 1D model and, in this respect, are much easier to implement. Our preliminary numerical results show that they work very well, at least for a cylindrical geometry.

With the proposed numerical scheme and the use of the proposed absorbing boundary conditions, we were able to show that the Womersley profile (i.e. the analytical solution in the rigid case) is meaningful also in the compliant case, provided we properly account for the delay due to the propagation of information at finite speed. This can be of a particular ineterest in haemodynamics, since the Womersley profile is always taken as a possible reference solution for pulsatile flows.

Acknowledgments

The authors acknowledge the support of the EU Commission through the *Haemodel project* HPRN-CT-2002-00270 and of the Italian grant PRIN 2005 "Numerical Modeling for Scientific Computing and Advanced Applications ".

References

[1] Abraham R., Marsden J,. Ratiu T., Tensor analysis on manifold, Addison-Wesley, 1983.

[2] Anayiotos A.S., Jones S.A., Giddens D.P., Glagov S., Zarins C.K., Shear stress at a compliant model of the human carotid bifurcation, J. Biomech. Engng., 117 (2004), 98–106.

[3] Bernadou M., Méthodes d'éléments finis pour les problèmes de coques minces, Masson, 1994.

[4] Berger S.A., Flow in large blood vessels, in Contemporary Mathematics, 141, 1993.

[5] Bonet J., Wood R.D., Non linear continuum mechanics for finite element analysis, Cambridge Univ. Press, 1997.

[6] Causin P., Gereau J.F., Nobile F., Added-mass effect in the design of partitioned algorithms for fluid-structure problems, Comp. Meth. Appl. Mech. Eng., 194 (2005), 4506–4527.

[7] Deparis S., Discacciati M., Fourestey G., Quarteroni A., Fluid-structure algorithms based on Steklov-Poincaré operators, Comp. Meth. Appl. Mech. Eng., in press.

[8] Deparis S., Fernandez M.A., Formaggia L., Acceleration of a fixed point algorithm for a fluid-structure interaction using transpirations conditions, M2AN Math. Model. Num. Anal., 37(4) (2003), 601–616.

[9] Donea J., An arbitrary lagrangian-eulerian finite element method for transient dynamic fluid-structure interactions, Comp. Meth. Appl. Mech. Eng., 33 (1982), 689–723.

[10] Fernandez M.A., Gerbeau J.F., Grandmont C., A projection algorithm for fluid-structure interaction problems with strong added-mass effect, C. R. Acad. Sci. Paris., 342 (2006), 279–284.

[11] Fernandez M.A., Moubachir M., A Newton method using exact jacobians for solving fluid-structure coupling, Comp. and Struct., 83(2-3) (2005), 127–142 .

[12] Figueroa C.A., Vignon-Clementel I.E., Jansen K.E., Hughes T.J.R., Taylor C.A., A coupled momentum method for modeling blood flow in three-dimensional deformable arteries, Comp. Meth. Appl. Mech. Eng., 195(41-43) (2006), 5685–5706.

[13] Formaggia L., Gerbeau J.F., Nobile F., Quarteroni A., On the coupling of 3D and 1D Navier-Stokes equations for flow problems in compliant vessels, Comp. Meth. Appl. Mech. Eng., 191 (2001), 561–582.

[14] Formaggia L., Gerbeau J.F., Nobile F., Quarteroni A., Numerical treatment of Defective Boundary Conditions for the Navier-Stokes equation, SIAM J. Num. Anal., 40(1) (2002), 376-401.

[15] Formaggia L., Moura A., Nobile F., On the stability of the coupling of 3D and 1D fluid-structure interaction models for blood flow simulations, submitted.

[16] Formaggia, L., Nobile, F., A stability analysis for the arbitrary Lagrangian Eulerian formulation with finite elements, East-West J. Numer. Math., 7(2) (1999), 105–131.

[17] Formaggia L., Nobile F., Stability analysis of second-order time accurate schemes for ALE-FEM, Comput. Methods Appl. Mech. Eng., 193(39-41) (2004), 4097–4116.

[18] Formaggia L., Nobile F., Quarteroni A., Veneziani A., Multiscale modelling of the circulatory system: a preliminary analysis, Comp. Vis. Sc., 2 (1999), 75–83.

[19] Formaggia L., Quarteroni A., Mathematical Modelling and Numerical Simulation of the Cardiovascular System, in Modelling of Living Systems, Handbook of Numerical Analysis, Ayache N, Ciarlet PG, Lions JL (eds), Elsevier Science, Amsterdam, 2003.

[20] Formaggia L., Veneziani A., Reduced and multiscale models for the human cardiovascular system, Lecture Notes, VKI Lecture Series, 2003.

[21] Formaggia L., Veneziani A., Vergara C., A new approach to the numerical solution of defective boundary problems in incompressible fluid dynamics, MOX Report n. 89, also submitted.

[22] Forster C., Wall W., Ramm E., Artificial added mass instabilities in sequential staggered coupling of nonlinear structures and incompressible viscous flow, Comp. Meth. Appl. Mech. Eng., 196(7) (2007), 1278–1293.

[23] Fung Y.C., Biomechanics: machanical properties of living tissues, Springer-Verlag, New York, 1993.

[24] Gerbeau J.F., Vidrascu M., A quasi-Newton algorithm based on a reduced model for fluid structure problem in blood flows, M2AN Math. Model. Num. Anal., 37(4) (2003), 631–647.

[25] Glowinski R., Pan T.W., Periaux J., A fictitious domain method for external incompressible viscous flow modeled by Navier-Stokes equations, Comp. Meth. Appl. Mech. Eng., 112(1-4) (1994), 133–148.

[26] Grandmont C., Analyse mathematique et numerique de quelques problemes d'interaction fluide structure, Ph.D. Thesis, Universite Paris 6, 1998.

[27] Grandmond C., Maday Y., Fluid-structure interaction: a theoretical point of view, in Fluid-structure interaction, Innov. Tech. Series, Kogan Page Sci., London, 2003

[28] Haywood J.G., Rannacher R., Turek S., Artificial Boundary and Flux and Pressure Conditions for the Incompressible Navier-Stokes Equations, Int. Journ. Num. Meth. Fluids, 22 (1996), 325-352.

[29] Hecht F., Pironneau O., Le Hyaric F., Ohtsuka K., Freefem++, `www.freefem.org`.

[30] Hilbert, D., An efficient Navier-Stokes solver and its applications to fluid flow in elastic tubes, Colloquia Societatis Janos Bolyai, 50 (1987), 423–431.

[31] Hughes T.J.R., Liu W.K., Zimmermann T.K., Lagrangian-Eulerian finite element formulation for incompressible viscous flows, Comp. Meth. Appl. Mech. Eng., 29(3) (1981), 329–349.

[32] Koiter W.T., On the non-linear theory of thin elastic shells. Proc. Kon. Neder. Akad. Wet., B69 (1996), 1–54.

[33] Koiter W.T., On the foundations of the linear theory of thin elastic shells, Proc. Kon. Neder. Akad. Wet., B73 (1970), 169–195.

[34] Lang S., Introduction to differentiable manifold, N.Y.-Wiley Interscience, 1962

[35] Le Tallec P., Mouro J., Fluid structure interaction with large structural displacements, Comp. Meth. Appl. Mech. Eng., 190 (2001), 3039–3067.

[36] H. Matthies, J. Steindorf, Numerical effciency of different partitioned methods for fluid-structure interaction, Z. Angew. Math. Mech., 2(80) (2000), 557–558.

[37] Maurits N.M., Loots G.E., Veldman A.E.P, The influence of vessel wall elasticity and peripheral resistance on the flow wave form: a CFD model compared to in-vivo ultrasound meaurements, J. Biomech., available online, 2006.

[38] Mittal S., Tezduyar T.E., Parallel finite element simulation of 3D incompressible flows: fluid-structure interactions, Int. J. Numer. Methods Fluids, 21 (1995), 933–953.

[39] Nobile F., Numerical Approximation of Fluid-Structure Interaction Problems with Application to Haemodynamics, Ph.D. Thesis, EPFL, Lausanne, 2001.

[40] Pedley T.J., The fluid mechanics of large blood vessels, Cambridge University Press, Cambridge, 1980.

[41] Perktold K., Rappitsch G., Mathematical modeling of local arterial flow and vessel mechanics. In Crolet, J., Ohayon, R. (eds.) Computational Methods for Fluid Structure Interaction, Pitman Research Notes in Mathematics, 306, 230–245, Harlow Longman, 1994.

[42] Peskin C.S., McQueen D.M., A three dimensional computational method for blood flow in the hearth - I Immersed elastic fibers in a viscous incompressible fluid, J. Comp. Phys., 81(2) (1989), 372–405.

[43] Quarteroni A., Tuveri M., Veneziani A., Computational Vascular Fluid Dynamics: Problems, Models and Methods, Computing and Visualisation in Science, 2 (2000), 163-197.

[44] Quarteroni A., Valli A., Numerical Approximation of Partial Differential Equations, Springer, 1994.

[45] Quarteroni A., Veneziani A., Analysis of a geometrical multiscale model based on the coupling of ODE's and PDE's for blood flow simulations, SIAM Multiscale Models Simulation, 1(2) (2003), 173-195.

[46] Veneziani A., A Mathematical and Numerical modeling of blood flow problems, Ph.D. thesis, University of Milan, 1998.

[47] Veneziani A., Vergara C., Flow rate defective boundary conditions in haemodinamics simulations, Int. Journ. Num. Meth. Fluids, 47 (2005), 803-816.

[48] Veneziani A., Vergara C., An approximate method for solving incompressible Navier-Stokes problem with flow rate conditions, Comp. Meth. Appl. Mech. Eng., in press.

[49] Vergara C., Numerical modeling of defective boundary problems in incompressible fluid-dynamics - Applications to computational haemodynamics, Ph.D. thesis, Politecnico di Milano, 2006.

[50] Womersley J.R., Oscillatory motion of a viscous liquid in a thin-walled elastic tube: I. The linear approximation for long waves, Philosophical Magazine, 46, 199-221, 1955.